ASTHMA

Oncostatin M expression induced by bacterial triggers drives airway inflammatory and mucus secretion in severe asthma

**Sarah E. Headland[1], Hart S. Dengler[1], Daqi Xu[1], Grace Teng[1], Christine Everett[2], Rojo A. Ratsimandresey[1], Donghong Yan[3], Jing Kang[3], Kirthana Ganeshan[1], Evgeniya V. Nazarova[1], Sarah Gierke[4,5], Christopher J. Wedeles[1], Riccardo Guidi[1], Daryle J. DePianto[1], Katrina B. Morshead[1], Alison Huynh[6], Jessica Mills[6], Sean Flanagan[6], Shannon Hambro[6], Victor Nunez[6], Joanna E. Klementowicz[7], Yongchang Shi[2], Jianyong Wang[2], Jack Bevers III[8], Vladimir Ramirez-Carrozzi[1], Rajita Pappu[1], Alex Abbas[9], Jason Vander-Heiden[9], David F. Choy[10], Rajbharan Yadav[11], Zora Modrusan[12], Reynold A. Panettieri Jr.[13], Cynthia Koziol-White[13], William F. Jester Jr.[13], Brendan J. Jenkins[14,15], Yi Cao[9], Christine Clarke[9], Cary Austin[5], Daniel Lafkas[1], Min Xu[3], Paul J. Wolters[16], Joseph R. Arron[1], Nathaniel R. West[7], Mark S. Wilson[1]*

Exacerbations of symptoms represent an unmet need for people with asthma. Bacterial dysbiosis and opportunistic bacterial infections have been observed in, and may contribute to, more severe asthma. However, the molecular mechanisms driving these exacerbations remain unclear. We show here that bacterial lipopolysaccharide (LPS) induces oncostatin M (OSM) and that airway biopsies from patients with severe asthma present with an OSM-driven transcriptional profile. This profile correlates with activation of inflammatory and mucus-producing pathways. Using primary human lung tissue or human epithelial and mesenchymal cells, we demonstrate that OSM is necessary and sufficient to drive pathophysiological features observed in severe asthma after exposure to LPS or *Klebsiella pneumoniae*. These findings were further supported through blockade of OSM with an OSM-specific antibody. Single-cell RNA sequencing from human lung biopsies identified macrophages as a source of OSM. Additional studies using *Osm*-deficient murine macrophages demonstrated that macrophage-derived OSM translates LPS signals into asthma-associated pathologies. Together, these data provide rationale for inhibiting OSM to prevent bacterial-associated progression and exacerbation of severe asthma.

INTRODUCTION

Asthma is an increasingly common respiratory disease with patients experiencing episodic acute exacerbations of disease with varying degrees of inflammation, mucus hypersecretion, reversible airflow obstruction, and airway hyperresponsiveness. The exact triggers and underlying molecular mechanisms causing acute exacerbations remain poorly defined, although viruses, bacteria, environmental toxins, ozone, and allergens are believed to contribute to acute exacerbations and progressive worsening of disease. About half of patients with asthma develop type 2 cytokine-driven inflammation (*1*); most molecularly targeted therapeutic interventions target these pathways, including interleukin-4 (IL-4) receptor (IL-4R), IL-5, IL-13, and immunoglobulin E (IgE) (*2*–*5*). In contrast, very few treatment options are available for patients with non–type 2 asthma, beyond nonspecific treatments such as inhaled corticosteroids and β-adrenergic agonists. Identifying triggers of disease exacerbation, the molecular consequences of exposure to such triggers, and points of therapeutic intervention to prevent hyperreactivity to such triggers could address a remaining unmet need for patients living with asthma (*6*, *7*).

Over the past decade, our appreciation and understanding of microbial symbionts inhabiting healthy airways have grown to the point where bacterial dysbiosis has been identified in patients with a variety of airway diseases, including asthma (*8*). The quantity and quality of bacterial components are often altered in individuals with severe asthma, both during stable disease (*9*–*11*) and particularly in patients experiencing exacerbations (*12*). It remains unclear whether dysbiosis per se contributes to increased cellular activation; however, these observations have led to the hypothesis that bacteria contribute to disease exacerbations. If so, the molecular pathways triggered by bacterial components in the airways of patients with asthma remain poorly defined. In addition to triggering exacerbations, bacterial components may also contribute to the development and progression of disease because many allergens contain bacterial-derived ligands including lipopolysaccharide (LPS) (*13*),

[1]Immunology Discovery,Genentech Inc., South San Francisco, CA 94080, USA. [2]Biochemical and Cellular Pharmacology, Genentech Inc., South San Francisco, CA 94080, USA. [3]Translational Immunology, Genentech Inc., South San Francisco, CA 94080, USA. [4]Center for Advanced Light Microscopy, Genentech Inc., South San Francisco, CA 94080, USA. [5]Pathology, Genentech Inc., South San Francisco, CA 94080, USA. [6]Necropsy, Genentech Inc., South San Francisco, CA 94080, USA. [7]Cancer Immunology Discovery, Genentech Inc., South San Francisco, CA 94080, USA. [8]Antibody Discovery, Genentech Inc., South San Francisco, CA 94080, USA. [9]OMNI Bioinformatics, Genentech Inc., South San Francisco, CA 94080, USA. [10]Biomarker Discovery OMNI, Genentech Inc., South San Francisco, CA 94080, USA. [11]Preclinical and Translational Pharmacokinetics and Pharmacodynamics, Genentech Inc., South San Francisco, CA 94080, USA. [12]Molecular Biology, Genentech Inc., South San Francisco, CA 94080, USA. [13]Rutgers Institute for Translational Medicine and Science, State University of New Jersey, New Brunswick, NJ 08901, USA. [14]Centre for Innate Immunity and Infectious Diseases, Hudson Institute of Medical Research, Clayton, Victoria, Australia. [15]Department of Molecular Translational Science, Faculty of Medicine, Nursing, and Health Sciences, Monash University, Clayton, Victoria 3800, Australia. [16]Division of Pulmonary, Critical Care, Allergy, and Sleep Medicine, Department of Medicine, University of California, San Francisco, San Francisco, CA 94110, USA.
*Corresponding author. Email: wilson.mark@gene.com

and Toll-like receptor 4 (TLR4)–binding proteins are a constituent of the common aeroallergen, house dust mite (HDM) (*14*). Preclinical models of asthma support this notion, because bacterial ligands and host recognition receptors are both required for allergen-induced airway inflammation (*15*, *16*). However, the underlying host responses that translate bacterial triggers into asthma-associated pathologies have remained elusive. Understanding and therapeutically targeting bacterial driven pathways may therefore provide benefit to patients by reducing disease development, progression, and bacterial-driven exacerbations. The major bacterial-derived component, LPS, has been extensively studied, from its initial binding to LPS-binding proteins (*17*), formation of CD14:TLR4:myeloid differentiation factor 2 complexes (*18*, *19*), recruitment of a variety of intracellular adaptor proteins, signaling transduction cascades, and transcriptional responses (*20*). Much focus has been given to LPS-induced proinflammatory mediators, such as IL-1α, IL-1β, tumor necrosis factor–α (TNF-α), and IL-8 (*21*); however, LPS induces a plethora of additional cytokines, including oncostatin M (OSM) (*22*).

OSM is member of the gp130 family of cytokines, and despite its contribution to a variety of physiological responses (*23*), it has been less intensively studied than its closely related family member, IL-6. Elevated concentrations of OSM have been frequently observed in allergic diseases (*24*–*26*), and OSM can stimulate a variety of responses in asthma-relevant epithelial and mesenchymal cells of the lung, including airway epithelial cells (*27*, *28*), fibroblasts (*29*, *30*), and airway smooth muscle cells (ASMs) (*31*, *32*). Both pro- and anti-inflammatory properties of OSM have been reported. For example, in the intestine of mice, OSM contributes to bacterial-driven inflammation and pathology (*33*), whereas anti-inflammatory properties of OSM have also been reported in models of arthritis and diabetic wound healing (*34*, *35*). These discrepancies may be explained by the use of recombinant human OSM in mice, which can bind to the murine leukemia inhibitory factor (LIF) receptor (*36*) instead of the dedicated OSM receptor β (OSMRβ). Whether OSM is a major driver of allergen- or bacterial-driven inflammation in the airways and whether targeting OSM would prevent bacterial-associated exacerbations remain unclear.

Here, we show that OSM is predicted to be a major driver of the transcriptional response observed in severe asthma. Using primary human epithelial and mesenchymal cells and human precision cut lung slices (PCLSs), we identify distinct OSM-induced inflammatory and mucus-producing pathways and provide evidence that OSM can drive a suite of goblet cell–associated genes, promote mucus production, and may compromise mucociliary clearance (MCC). Gain- and loss-of-function studies in murine models of asthma demonstrate that OSM is required for HDM-driven airway inflammation. Mechanistic studies identify that LPS-induced OSM from macrophages is both necessary and sufficient to translate bacterial-derived signals into proallergic responses. Using a model of *Klebsiella pneumoniae*, OSM blockade reduced airway neutrophilia and *Muc5ac*, *Muc5b*, and *Clca1* gene expression without compromising expression of *Il1a*, *Il1b*, and *Il6* or antibacterial immunity. Although experimental *K. pneumoniae* infection does not model dysbiosis, it illustrates an important role of bacterial-driven OSM contributing to pathology rather than immunity. Together, these data identify OSM as an important contributor to airway inflammation and mucus hypersecretion and support the therapeutic hypothesis that blocking OSM could prevent disease progression and bacterial-associated exacerbations without compromising antibacterial immunity.

RESULTS

OSM:OSMR signaling is elevated in patients with severe asthma

Bronchial airway epithelial cells (BAECs), which sit at the interface between the host and environment, have been useful sentinels for classifying asthma heterogeneity (*37*), characterizing disease severity (*38*), and establishing predictive biomarkers (*39*). We took advantage of these properties and performed a post hoc analysis of the transcriptome derived from bronchial brushings recovered from 16 healthy volunteers, 28 individuals with mild-to-moderate asthma (mild/mod), and 57 individuals with severe asthma (severe) (*37*, *39*–*41*) to identify molecular pathways enriched in severe asthma (table S1). We used an upstream analysis algorithm (*42*) to identify putative regulators of the observed transcriptome in individuals with severe asthma, relative to mild/mod and healthy control transcriptomes (table S2). This analysis identified steroids and steroid-induced genes [dexamethasone, fluticasone propionate, and FKBP prolyl isomerase 5 (FKBP5) (*43*)], cytokines and cytokine receptor signaling pathways [IL-13, transforming growth factor–β, amphiregulin, signal transducer and activator of transcription 1 (STAT1) and STAT4, IL-1A, and IL-1R1], and erythropoietin as factors that could contribute to the observed transcriptome in bronchial brushings obtained from individuals with severe asthma (Fig. 1A and fig. S1A). However, OSM was the most significant ($P < 0.01$) predicted upstream regulator contributing to differential gene expression in bronchial brushings from individuals with severe asthma. OSM itself was not expressed in epithelial cells; however, in line with an OSM-driven response, *OSMR*, which is up-regulated by OSM along with several other gp130-dependent cytokine receptors, *IL27RA*, *IL11RA*, and *GP130* (*IL6ST*) (Fig. 1B and fig. S1A), was differentially expressed in individuals with severe asthma. IL-33, an early and potent epithelial-derived inflammatory mediator observed in severe asthma (*44*, *45*) and also regulated by OSM (*46*), correlated with elevated *OSMR* in severe, but not mild/mod, asthma or healthy controls (Fig. 1C). Similarly, *MUC5AC*, *MUC2*, and *SPDEF*, a transcriptional regulator of goblet cell differentiation and mucus hypersecretion, a major pathology observed in severe asthma (*47*, *48*), were up-regulated in individuals with severe asthma (fig. S1B) and correlated with elevated OSMR in severe, but not mild/mod, asthma or healthy controls (Fig. 1D). Although the cellular composition of the bronchial brushings may vary between individuals with different degrees of asthma severity, collectively, these data point toward a role for the OSM:OSMR axis in severe asthma, correlating with genes involved in inflammatory and mucus-producing pathologies.

OSM drives inflammatory and mucus-producing pathways in human mesenchymal and epithelial cells, respectively

To identify OSM-induced pathogenic pathways and biomarkers in primary human disease-relevant cells of the lung, we cultured human BAECs grown at air-liquid interface (BAEC-ALI), normal human lung fibroblasts (NHLFs) in a three-dimensional (3D) matrix, and human ASMs in collagen rafts and stimulated these cells with recombinant OSM (rOSM). rOSM treatment led to phosphorylation of STAT3, STAT4, and STAT5 within 15 min, albeit to varying degrees depending on cell type (Fig. 2, A to C). After 6 hours, substantial transcriptional activity was observed (Fig. 2D), and although each cell type responded to OSM, cell type–specific responses were clearly distinguishable. ASM and NHLF shared more OSM-induced responses (22.4% in common, 107 of 370) than either cell type shared

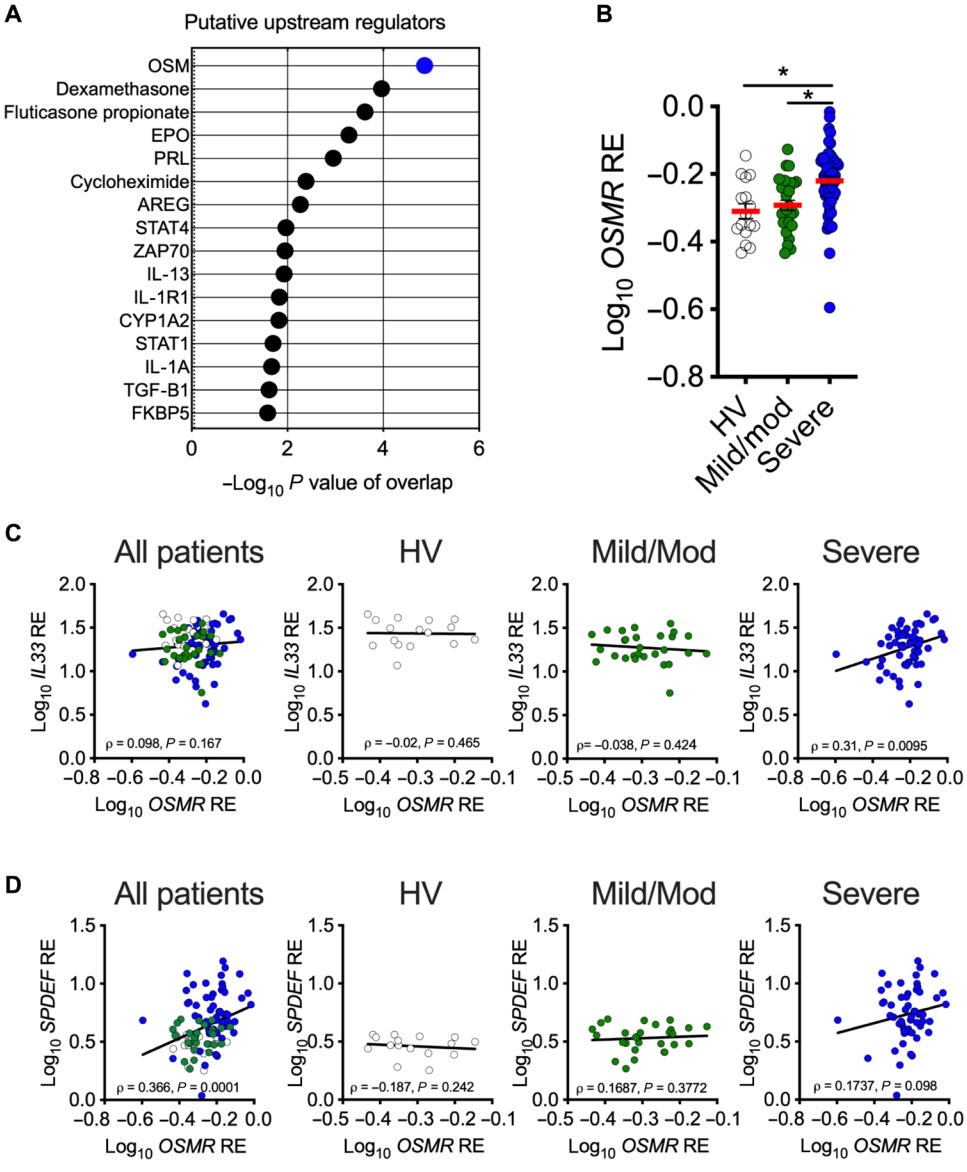

Fig. 1. An OSM:OSMR axis correlates with *IL33* and *SPDEF* expression in severe asthma. (**A**) Transcriptional data from bronchial airway epithelial brushings isolated from healthy volunteers (HVs), patients with mild-to-moderate asthma (mild/mod), or patients with severe asthma (severe), previously described (*37*, *39*, *41*), were analyzed using Ingenuity Pathway Analysis (IPA) to identify putative upstream regulators. OSM is highlighted in blue. (**B**) Expression of *OSMR* is shown for bronchial airway epithelial brushings isolated from healthy volunteers, patients with mild/mod, or patients with severe asthma (severe). Data presented as $\log_{10}$ relative expression (RE). Data are presented as means ± SEM. Data were analyzed by ANOVA with Dunnett's multiple comparison correction. *$P < 0.05$. (**C** and **D**) Correlation between OSMR and *IL33* (C) or *SPDEF* (D) is shown for bronchial airway epithelial brushings isolated from healthy volunteers, patients with mild/mod, or patients with severe asthma (severe). Spearman correlation (ρ) values and *P* values are displayed on figures.

with BAEC (BAEC and ASM, 7%, 28 of 374; BAEC and NHLF, 4.4%, 21 of 455) (Fig. 2E), suggesting that OSM may have divergent functions in epithelial cells compared to mesenchymal cells. For example, haptoglobin (*HP*) and osteopontin (*SPP1*), which have both been correlated with severity of asthma (*49*, *50*), were up-regulated in BAEC but not in ASM or NHLF. In contrast, several inflammatory cytokines and chemokines, such as *CXCL10*, *CCL7*, *IL24*, and *CCL11*, were up-regulated in NHLF and ASM but not in BAEC. In contrast, OSM-induced *IL33* and histamine receptor (*HRH1*), both involved in asthma pathogenesis, were observed in all three cell types tested (Fig. 2F).

To further explore the response of airway epithelial cells to OSM, we treated BAEC-ALI with a single pulse of OSM and monitored the histological and transcriptional responses for 14 days. From day 3 onward, mucus-producing cells were clearly evident with an accumulation of mucus and goblet cells throughout the 14-day period (Fig. 2G). Functionally, using a fluorescent bead tracking assay to assess MCC (*51*), OSM-treated BAEC-ALI, which had a significant increase in mucus ($P < 0.05$), had significantly reduced MCC ($P < 0.05$; fig. S1C), as indicated by reduced bead movement, suggesting that OSM-driven mucus may compromise MCC. Between 6 and 72 hours, OSM induced expression of *IL33*, *SPP1*, and *HP* expression, all of which have been observed in severe asthma under steady-state or during acute exacerbations (*49*, *52*) (Fig. 2H). Similarly, cytokine and histamine receptors were up-regulated and sustained for 3 days after a single pulse of OSM. OSM stimulation up-regulated *MUC5AC*, *OSMR*, and *SPDEF* at 6 hours, in line with observations made in ex vivo bronchial brushings from individuals with severe asthma (Figs. 2H and 1D). From 6 hours onward, a suite of genes associated with goblet cell differentiation (*MUC5B*, *BPIFB1*, *MUC1*, and *MUC4*) were induced, providing a molecular explanation for the elevated mucus observed throughout the 14-day culture period (Fig. 2G). These data provide clear evidence that OSM is sufficient to initiate a plethora of responses in primary human airway epithelial and mesenchymal cells, including an inflammatory axis with induction of cytokines and chemokines, a tissue priming response with increased cytokine and histamine receptors in both epithelial and mesenchymal cells, and a mucus-producing program within the airway epithelium, driving goblet cell differentiation and mucus production.

OSM exacerbates allergen-driven airway inflammation

OSM and other members of the IL-6 family bind to and mediate signaling cascades in cells expressing gp130, one of two receptor chains required for OSM-mediated signaling, along with OSMR. To determine whether gp130-mediated signaling regulates responsiveness to the common HDM allergen, we sourced gain-of-function

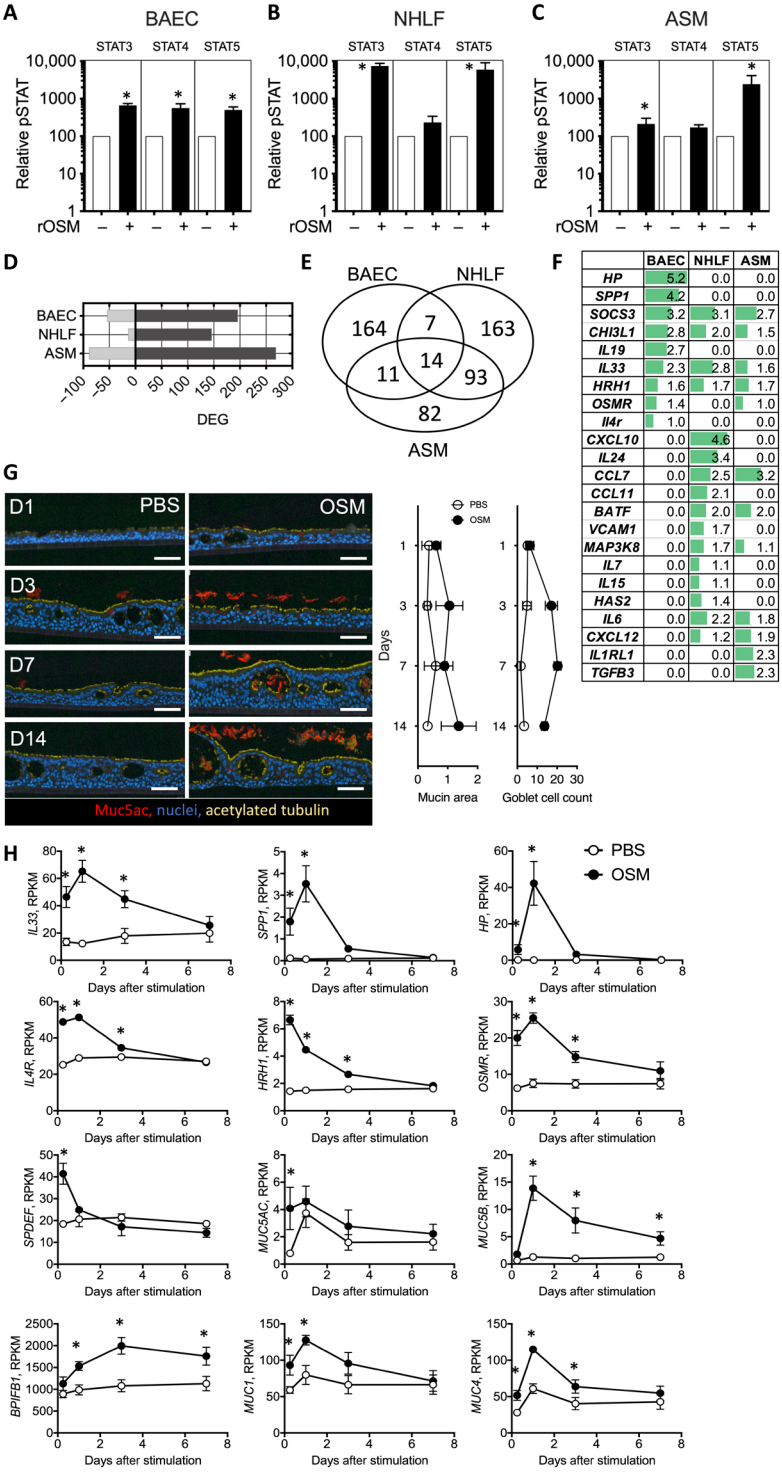

Fig. 2. OSM drives inflammatory and mucus-producing pathways in human epithelial and mesenchymal cells. (**A** to **C**) Primary human bronchial airway epithelial cells (BAECs) grown at an air-liquid interface (ALI). (A) Primary normal human lung fibroblasts (NHLFs) grown in three-dimensional (3D) rafts (B) and primary human ASMs grown in Matrigel (C) were stimulated with recombinant OSM (rOSM) for 15 min. Whole-cell lysates were extracted and probed for phosphorylated STAT3 (pSTAT3), pSTAT4, or pSTAT5. pSTAT expression is shown relative to unstimulated cells with five donors per cell type. Data are presented as means ± SD. (**D**) The number of differentially expressed genes (DEGs) ($P < 0.05$) observed in BAEC, NHLF, and ASMs with and without treatment with rOSM is shown. (**E**) A Venn diagram shows common and unique DEGs in indicated cell types. (**F**) Transcripts of DEGs [$\log_2$ fold change (FC), relative to PBS treated, $P < 0.05$] are shown with green bars proportional to FC value. Data in (D to F) were obtained from RNA-seq of primary human BAECs, NHLFs, and primary human ASMs after rOSM stimulation for 6 hours and represent five donors per cell type. (**G**) Primary human BAECs grown at an ALI and stimulated with rOSM for indicted time (days) are shown. Mucin area and goblet cell count were quantified by microscopy. Red, Muc5ac; blue, nuclei; yellow, ciliated cells. Scale bar, in all plots, 100 μm. Data are presented as means ± SEM. (**H**) Expression of genes is shown at indicated times after stimulation with rOSM. Data were obtained by RNA-seq of BAEC grown at an ALI with five donors per time point. Data are presented as means ± SEM. Data were analyzed using *t* tests at each time point. *$P < 0.05$. Reads Per Kilobase Million (RPKM).

gp130$^{F/F}$ mice, which are hyperresponsive to all gp130-dependent cytokines by virtue of phenylalanine knock-in substitution at tyrosine (F) 757 in the cytoplasmic domain of gp130 that prevents suppressor of cytokine signaling 3 (SOCS3)–mediated negative regulation (*53*) (fig. S2A). HDM sensitization and challenge of mice carrying the *gp130*^{Y757F} mutation accumulated significantly more HDM-induced granulocytic and lymphocytic infiltrates in the airways, relative to wild-type (WT) littermates ($P = 0.03$; Fig. 3A). Accompanying the increased inflammatory cells in *gp130*$^{F/F}$ mice were elevated cytokines (IL-4, IL-5, and IL-13), granulocyte-recruiting chemokines and growth factors, C-C motif chemokine 11 (CCL11) and granulocyte colony-stimulating factor (G-CSF) (Fig. 3B), and elevated expression of *Muc5ac* and *Muc5b* (fig. S2B). Collectively, these data indicate that gp130-dependent signaling, including but not exclusive to OSM, can exacerbate HDM-induced airway inflammation.

HDM treatment of WT mice increased expression of *Osm* in the lung and up-regulated *Osmr* in CD45$^-$CD31$^-$ epithelial cell adhesion molecule–positive (EpCAM$^+$) BAECs (fig. S2C), similar to observations made in epithelial brushings from individuals with severe asthma (Fig. 1A) and in BAEC-ALI cultures treated with OSM (Fig. 2, F and H). Furthermore, *Gp130*$^{F/F}$ mice, which are hyperresponsive to all gp130-dependent cytokines, mounted a greater response to HDM. To formally test whether OSM could exacerbate airway inflammatory responses, we exposed mice to HDM supplemented with rOSM (fig. S2D). Adding rOSM to HDM amplified airway inflammation and significantly increased airway granulocytes (eosinophils and neutrophils), lymphocytes ($P < 0.05$; Fig. 3C), bronchoalveolar lavage (BAL) cytokines (IL-5, IL-13, and IL-6), and the granulocyte chemokines and growth factors CCL11 and G-CSF ($P < 0.05$; Fig. 3D). These data support previous reports demonstrating that adenovirus-driven overexpression of OSM can invoke cardinal features of airway allergy (*54*).

Similar to observations made in epithelial brushings from individuals with severe asthma (Fig. 1A) and in BAEC-ALI cultures

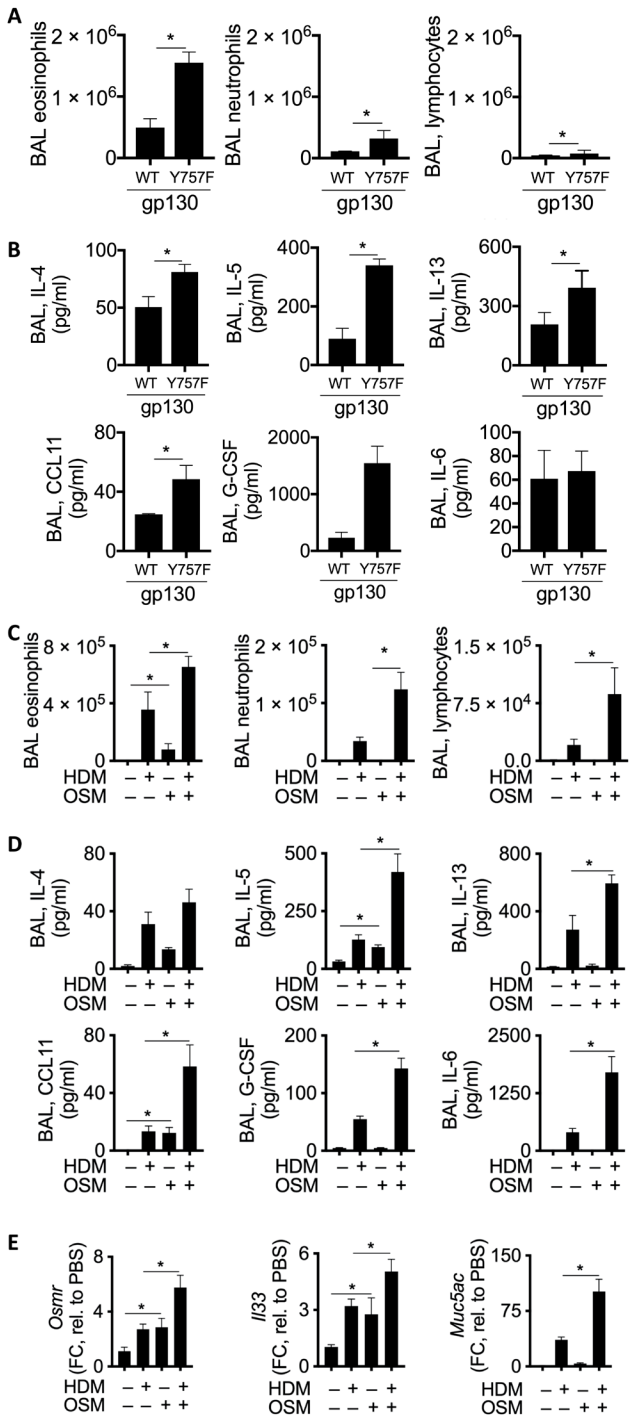

Fig. 3. Exogenous OSM exacerbates murine HDM-induced airway inflammation. (**A** and **B**) C57BL/6 *gp130*$^{F/F}$ or *gp130*$^{WT/WT}$ mice were treated with house dust mite (HDM; 10 μg in 25 μl) by the intratracheal route on days 0, 3, 7, 10, and 14 and analyzed on day 15 for bronchoalveolar lavage (BAL) fluid infiltrates (A) and BAL cytokine and chemokine secretions (B). $n = 5$ mice per group, one of three representative experiments is shown. (**C** to **E**) C57BL/6 mice were treated with HDM (10 μg in 25 μl) on days 0, 3, and 7 followed by HDM (10 μg in 25 μl) with or without rOSM (50 ng) on days 10 and 14, as indicated. Additional control mice were treated with rOSM (50 ng) on days 10 and 14 only, by the intratracheal route. Mice were analyzed on day 15 for BAL cellular infiltrates (C), BAL cytokine and chemokine secretions (D), and *Osmr*, *Il33*, and *Muc5ac* gene expression in whole lung tissue (E). Data in (E) are presented as FC relative to PBS-treated mice. $n = 5$ mice per group, one of two representative experiments is shown. Data are presented as means ± SEM. Data were analyzed using Mann-Whitney tests. *$P < 0.05$.

treated with OSM (Fig. 2, F and H), OSM-supplemented HDM led to greater *Osmr*, *Il33*, and *Muc5ac* expression in the lung (Fig. 3E). rOSM alone was sufficient to invoke airway infiltration of eosinophils, with accompanying increases in IL-5 and CCL11 in BAL and increased expression of *Osmr* and *Il33*. HDM-specific recall responses in local draining lymph nodes remained largely unaltered, suggesting that OSM-amplified responses were largely restricted to the lung, with little impact on T cell–derived cytokines (fig. S2E). These data support an OSM:OSMR axis contributing to a more severe form of airway inflammation and asthma, with evidence of both OSM-exacerbated inflammatory and mucus-producing responses in the airways.

Osm is required for allergen-driven airway inflammation and bacterial ligand–exacerbated airway inflammation

Several reports have identified elevated concentrations of OSM in biofluids and biopsies from patients with asthma (*26*) and elevated concentrations of OSM in preclinical airway inflammation models (*55*). As we show above, exogenous OSM can amplify allergen-induced airway inflammation; however, whether endogenous OSM is necessary for allergen-induced airway inflammation is unclear. We therefore asked whether OSM was required for HDM-induced airway inflammation using *Osm*$^{-/-}$ mice. After HDM exposure, *Osm*$^{-/-}$ mice had significantly fewer inflammatory cells in their airways ($P < 0.05$; Fig. 4A) and reduced secretion of airway cytokines ($P < 0.05$; Fig. 4B), compared to *Osm*-sufficient WT littermates. In agreement with the observation that OSM-induced *MUC5AC*, *MUC5B*, and *IL33* in human airway epithelial cells (Fig. 2H), *Osm*$^{-/-}$ mice had significantly reduced expression of *Muc5ac*, *Muc5b*, and *Il33* in lung tissue ($P < 0.05$; Fig. 4C), indicating that OSM is a critical component of the HDM-driven response.

Bacterial components can induce OSM (*22*), which led us to hypothesize that OSM could be an important conduit translating bacterial triggers into more severe airway inflammatory responses. The presence of bacterial LPS in HDM could explain some of these results (*13*); however, we formally tested this hypothesis using LPS-supplemented HDM-induced airway inflammation, to better model bacterial-associated exacerbations and severe disease. Briefly, mice were sensitized to HDM by the intratracheal airway exposure, followed by HDM and LPS airway challenges. As expected, we observed severe airway inflammation, with a robust neutrophilic influx, accompanied by 5 to 10% eosinophils and lymphocytes (Fig. 4D), reflective of severe human asthma (*56*). Under these more severe conditions, *Osm*$^{-/-}$ mice were protected to an even greater degree (about 80% reduction in BAL neutrophils, compared to about 55% reduction in eosinophils in HDM model without LPS supplementation), with significantly fewer infiltrating neutrophils, eosinophils, lymphocytes, and BAL cytokines in *Osm*$^{-/-}$ mice ($P < 0.05$; Fig. 4D). This treatment regimen also led to the secretion of IL-6, G-CSF, and C-X-C motif chemokine ligand 10 (CXCL10) into the airways, all of which were dependent on OSM (Fig. 4E). These cytokine and chemokines were also directly inducible by OSM in BEAC-ALI cultures in vitro (Fig. 2F), suggesting that HDM/LPS induction of OSM was contributing to these responses. These data support the thesis

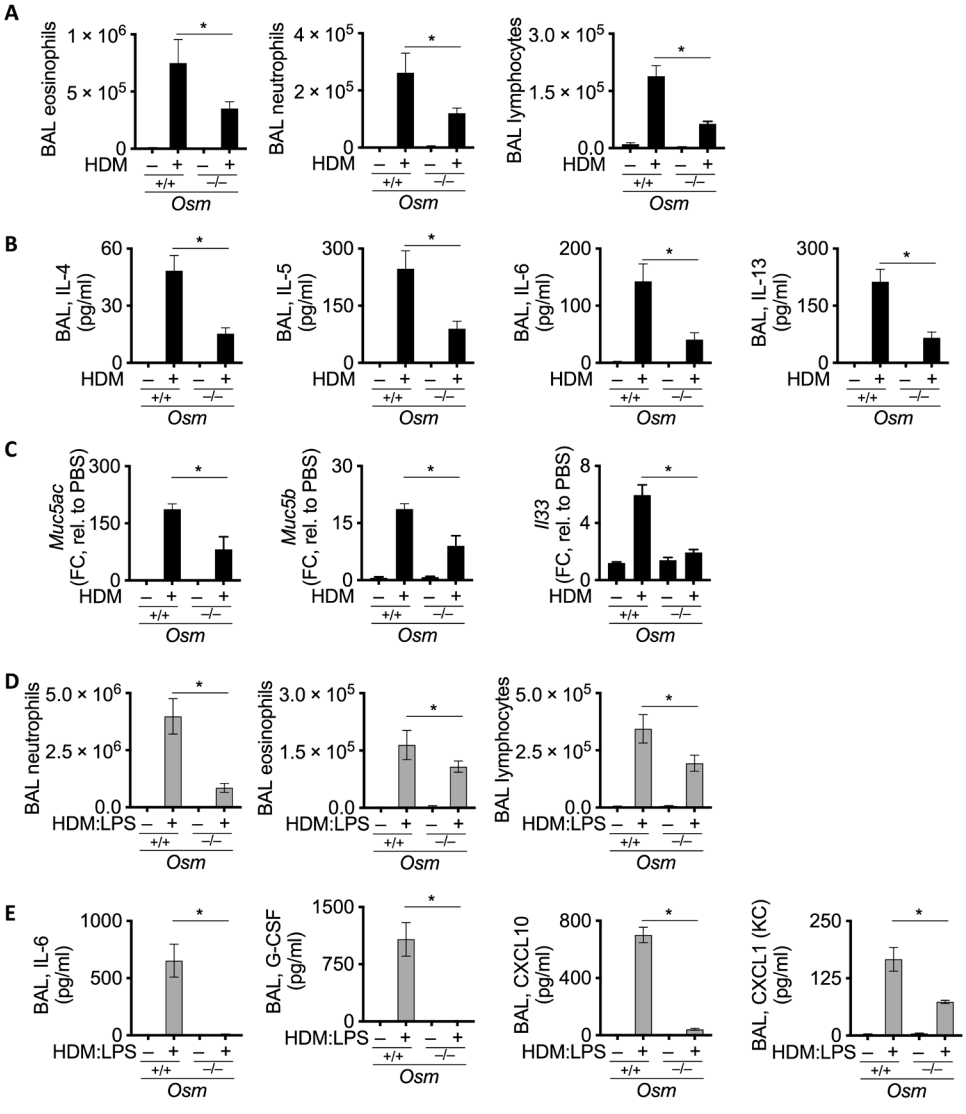

Fig. 4. *Osm* deficiency protects mice from type 2 (eosinophilic) and type 1 (neutrophilic) HDM-induced airway inflammation. (**A** to **C**) C57BL/6 *Osm*$^{-/-}$ or C57BL/6 WT mice were treated with intratracheal HDM (10 μg in 25 μl) on days 0, 2, 4, 14, 16, 28, and 30 and analyzed on day 31 for BAL cellular infiltrates (A), BAL cytokine and chemokine secretions (B), and *Muc5ac*, *Muc5b*, and *Il33* gene expression in whole lung tissue (C). $n = 5$ mice per group, one of three representative experiments is shown. *$P < 0.05$. (**D** and **E**) C57BL/6 *Osm*$^{-/-}$ or C57BL/6 WT mice were treated with intratracheal HDM (10 μg in 25 μl) supplemented with LPS (5 μg per mouse) on days 0, 2, 4, 14, 16, 28, and 30 and analyzed on day 31 for BAL infiltrates (D) and BAL cytokine and chemokine secretions (E). $n = 5$ mice per group, one of three representative experiments is shown. Data are presented as means ± SEM. Data were analyzed using Mann-Whitney tests; *$P < 0.05$. Keratinocytes-derived chemokine (KC).

that OSM is an important component of allergen-driven and bacterial-associated severe airway inflammation.

A potent anti-OSM blocking antibody prevents allergen-driven airway inflammation and bacterial ligand–exacerbated airway disease

The observations in *Osm*$^{-/-}$ mice prompted us to develop an anti-OSM blocking antibody (24.A8) to test whether therapeutic blockade of OSM in mice with established airway disease could reduce further allergen-driven inflammation. The hybridoma-derived antibody 24.A8 was generated by immunizing hamsters with murine OSM, and then the molecularly cloned antibody was reformatted into murine IgG2a for further studies. Binding kinetics were determined using surface plasmon resonance. Clone 24.A8, which had a fast on-rate and slow off-rate, had picomolar monovalent binding affinity for murine OSM (Fig. 5A). Using the mouse MLg fibroblast cell line, which is fully responsive to rOSM [half-maximal response; median effective concentration (EC_{50}); 2 ng/ml; Fig. 5B], we determined median inhibitory concentration (IC_{50}) values for 24.A8 in the 1 nM range (Fig. 5C). To test the pharmacodynamic (PD) properties of 24.A8, we treated mice with 24.A8 (20 mg/kg) by intraperitoneal injection, 24 hours before administering rOSM by the intratracheal route. We then measured phosphorylated STAT3 (pSTAT3) and pSTAT5 in whole lung tissue lysates 15 min after OSM treatment. At 20 mg/kg, 24.A8 completely blocked OSM-induced pSTAT3 and pSTAT5 (Fig. 5, D and E), highlighting the in vitro and in vivo potency of 24.A8. Pharmacokinetics (PKs) of 24.A8 were characterized after a single intravenous dose of 10 or 30 mg/kg in female C57BL/6 mice. 24.A8 demonstrated apparent biphasic distribution characterized by a rapid initial distribution phase followed by a slower elimination phase (Fig. 5F). Linear and dose-proportional [C_{max} and AUC (area under the concentration-time curve)] PKs were observed between 10 and 30 mg/kg, with clearance ranging from 2.9 to 3.5 ml/day per kilogram (table S3). After the favorable characterization of 24.A8 in vitro and in vivo, we tested the therapeutic potential of blocking OSM in mice with established HDM-driven and HDM/LPS-driven severe airway inflammation. As expected, HDM rechallenge induced significant airway eosinophilia ($P < 0.01$), whereas HDM/LPS rechallenge induced severe neutrophilic inflammation (Fig. 5, G and H). In both cases, blockade of OSM with 24.A8 before rechallenge with HDM or HDM/LPS significantly reduced granulocytic inflammation ($P < 0.05$; Fig. 5, G and H). Accompanying the reduction in airway granulocytes was a significant reduction in inflammatory cytokines and chemokines (IL-4, IL-5, IL-13, and CCL11 in HDM alone; IL-6, G-CSF, CXCL10, and CXCL1 in HDM/LPS) ($P < 0.05$; Fig. 5I and fig. S3). Collectively, these data indicate that OSM, whether endogenous, exogenous, or functional only during rechallenge, contributes to airway inflammation and more profoundly during bacterial endotoxin-exacerbated airway inflammation.

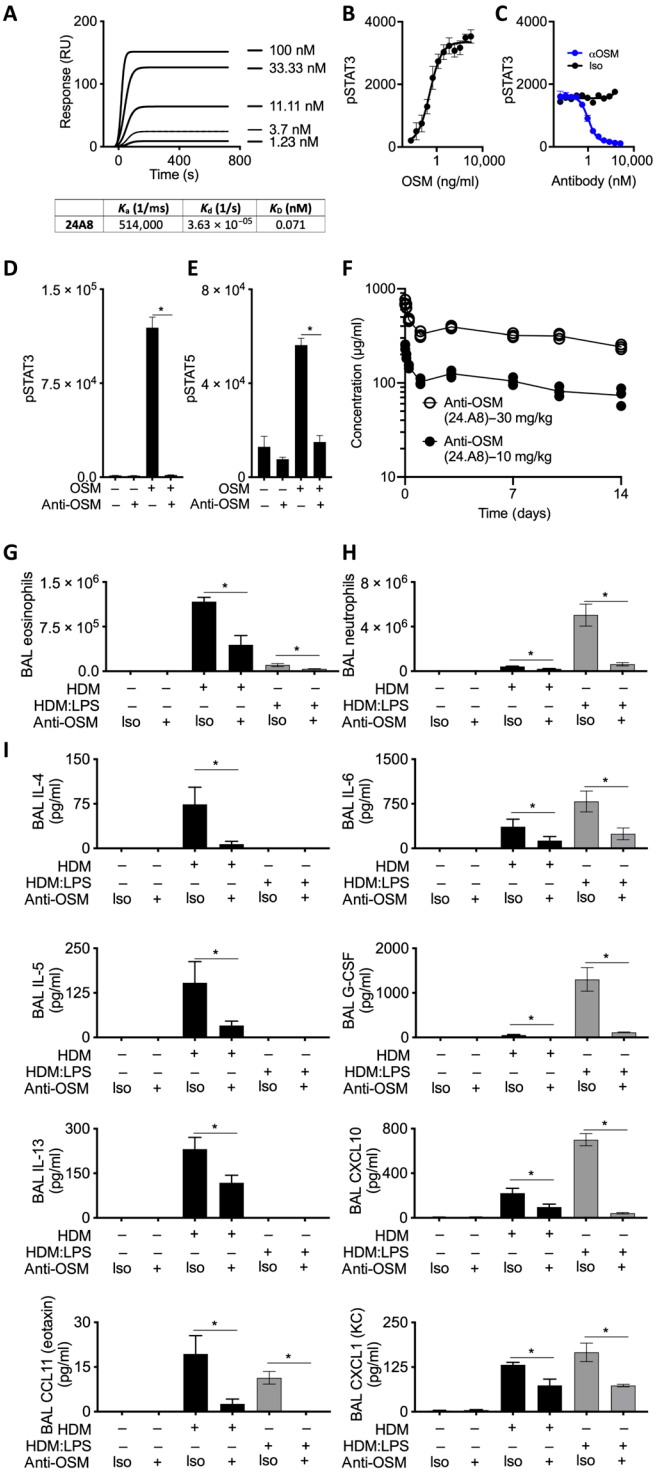

	K_a (1/ms)	K_d (1/s)	K_D (nM)
24A8	514,000	3.63×10^{-05}	0.071

Fig. 5. Anti-OSM antibody characterization, pharmacodynamics, pharmacokinetics, and efficacy. (**A**) Binding kinetics of anti-mouse OSM (24.A8) determined using surface plasmon resonance, showing fast on-rate (association, K_a), slow off-rate (dissociation, K_d), and picomolar monovalent binding affinity (K_D). Data are presented as relative units (RUs). (**B**) EC_{50} values for anti-OSM were determined in mouse MLg fibroblast cell lines stimulated with rOSM (EC_{50}, 2 ng/ml) by measuring pSTAT3. (**C**) IC_{50} values were determined for anti-OSM in mouse MLg fibroblast cell lines stimulated with rOSM (2.5 ng/ml). Iso indicates isotype control antibody. Data are presented as means ± SEM. (**D** and **E**) Pharmacodynamic (PD) properties of anti-OSM antibody were determined in mice treated with anti-OSM (20 mg/kg, ip) 24 hours before administering rOSM (50 ng in 25 μl) by the intratracheal route. pSTAT3 (D) and pSTAT5 (E) were measured in whole lung tissue lysates after 15 min. Data are presented as means ± SEM. Data were analyzed using Mann-Whitney test. (**F**) Pharmacokinetic (PK) properties of anti-OSM were characterized after a single intravenous dose of 10 or 30 mg/kg in female C57BL/6 mice. (**G** to **I**) C57BL/6 WT mice were treated with intratracheal HDM (10 μg in 25 μl) or HDM supplemented with LPS (5 μg per mouse), as indicted, on days 0, 2, 4, 14, 16, 28, and 30 and analyzed on day 31 for BAL infiltrates (G and H) and BAL cytokine and chemokine secretions (I). Mice were given an isotype control (Iso; 20 mg/kg, mouse anti-gp120) or anti-OSM on days 27 and 29, 1 day before HDM or HDM:LPS challenge. $N = 5$ mice per group, one of three representative experiments is shown. Data in (G) to (I) are presented as means ± SEM. Data were analyzed using Mann-Whitney tests. *$P < 0.05$.

OSM contributes to LPS-induced airway inflammation and drives broad inflammatory responses in tissue

Bacterial dysbiosis and bacterial components are frequently detected in individuals with severe asthma both during stable disease (*9*, *10*) and in patients suffering exacerbations of disease (*12*). In preclinical models, bacterial components and TLR4 are required for allergen-induced airway inflammation (*15*, *16*); however, the molecular mechanisms translating these microbial triggers into allergen-related airway disease remained unclear. The observations that OSM was required for both HDM-induced and, in particular, HDM/LPS-induced airway inflammation (Figs. 4 and 5) led us to test the hypothesis that OSM is a critical component that translates LPS exposure to asthma-like manifestations. We simplified the airway inflammation model to a single LPS exposure to test whether LPS induced OSM in vivo and, if so, the nature of OSM-dependent LPS responses. After acute LPS exposure, *Osm* was significantly increased in the lungs of WT, but not $Osm^{-/-}$, mice ($P < 0.01$; Fig. 6, A and B), validating this experimental setup. Transcriptional analysis of lung tissue at 4 hours after LPS exposure identified differences between in gene expression between WT and $Osm^{-/-}$ mice ($P < 0.05$; Fig. 6, C to F). The absence of *Osm* resulted in fewer differentially expressed genes (DEGs) (3624 DEGs in WT compared to 2118 DEGs in $Osm^{-/-}$; Fig. 6D), and although 1560 LPS-induced genes were unaffected by the absence of *Osm* (Fig. 6E and fig. S4), we identified 2064 DEGs that were OSM dependent (differentially regulated in WT, but not in $Osm^{-/-}$ mice) (Fig. 6F). Of particular note, LPS induced OSM-dependent inflammatory genes (*Il36a*, *Aldh1a3*, *Traf2*, *Crp*, *Ccr2*, *Ccr4 and Cxcr4*, *Il12rb*, *Il18r1*, and *Il1r1*), including many genes with a clear type 2, proallergic bias (*Il5*, *Il33*, *Il16*, *Il19*, *Il13ra2*, *Il31ra*, *Osm*, *Ccl17*, and *Gfi1*) (*57*), supporting the mechanistic explanation of LPS-induced OSM as an important component of an asthma-like response in the airways. Furthermore, airway delivered LPS-induced systemic responses, including serum G-CSF and IL-5, which were both significantly reduced in the absence of OSM ($P < 0.05$; fig. S4). Beyond inflammatory genes, LPS induced expression programs involved in nitric oxide signaling (*Hmga1*, *Ifgr2*, *Nos2*, *Ikbke*, *Jak1*, *Jak3*, *Ly96*, and *Stat1*), microbial recognition and responsiveness (*Tlr1*, *Tlr4*, *Tlr9*, and *Camp*, encoding cathelicidin antimicrobial peptide), and tissue injury and remodeling (*Col11a2*, *Col13a1*, *Col22a1*, *Pgf*, *Dio2*, *Muc4*, *Mmp3*, *Mmp14*, and *Adam17*) (Fig. 6F), all of which were dependent on OSM.

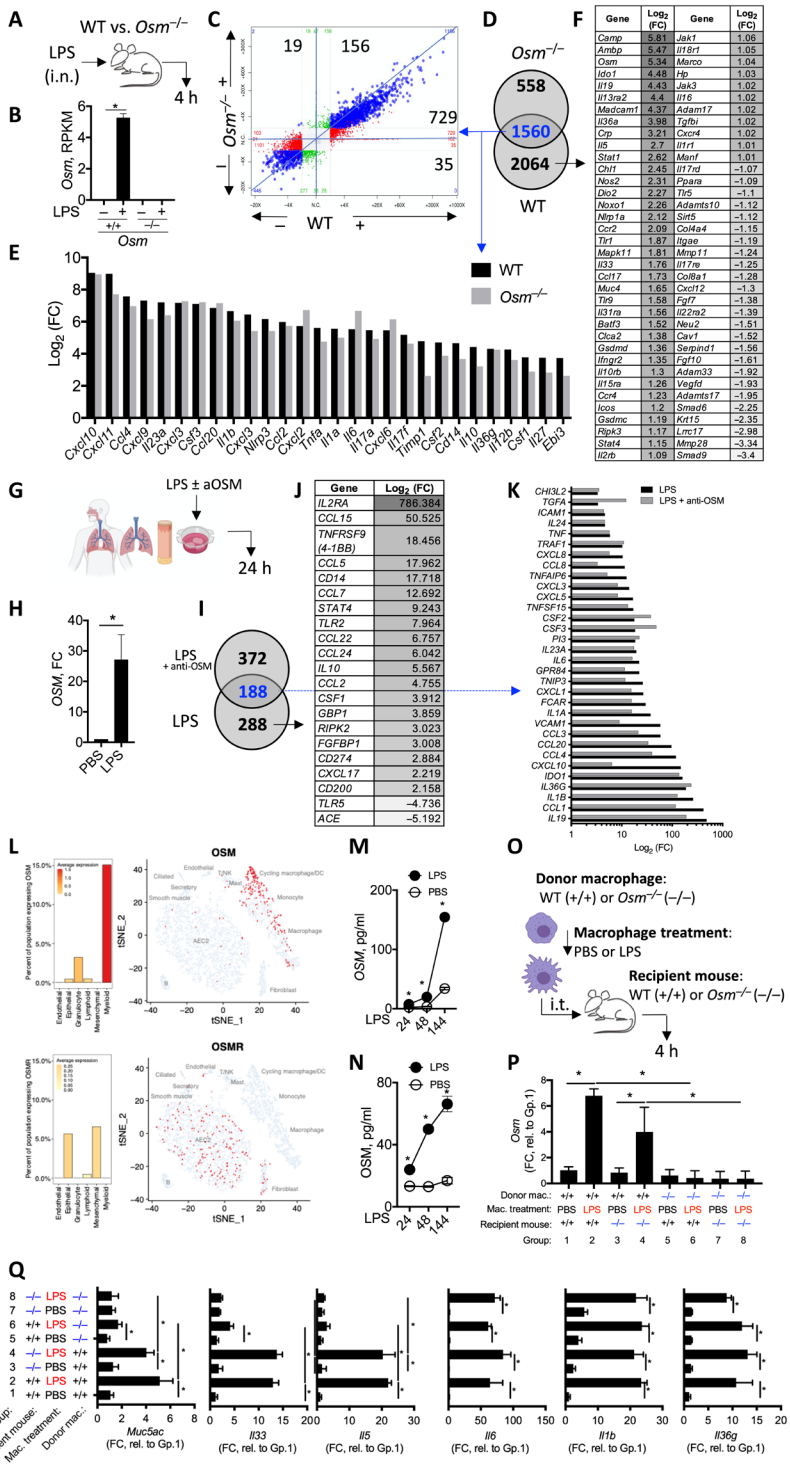

Fig. 6. OSM drives tissue inflammation after exposure to endotoxin signals. (**A**) C57BL/6 *Osm*$^{-/-}$ or C57BL/6 WT mice were given LPS (5 μg) by the intranasal (i.n.) route and LPS-induced responses measured after 4 hours. (**B** to **F**) Transcriptional responses in the lung after LPS treatment were determined by RNA-seq. (B) *Osm* expression in whole lung tissue is shown. Data are presented as means ± SEM. Data were analyzed using Mann-Whitney test. (C) DEGs in lung tissue from C57BL/6 *Osm*$^{-/-}$ or C57BL/6 WT mice after LPS treatment are shown. N.C., No change. (D) The Venn diagram showing common and unique DEGs in C57BL/6 *Osm*$^{-/-}$ or C57BL/6 WT mice. (E) Common and quantitative DEGs in lung tissue after LPS treatment are shown as FC values. (F) OSM-dependent DEG in lung tissue after LPS treatment is shown in the table. (**G**) Human precision cut lung slices (PCLSs) were stimulated with LPS in the presence of anti-human OSM-blocking antibody or an isotype control antibody. Three human PCLS donors were used with three technical replicates. (**H**) Induction of *OSM* in human PCLS is shown as FC relative to PBS-treated donor-matched PCLS. Data are presented as means ± SEM. Data were analyzed using paired *t* test. (**I** to **K**) Transcriptional responses in PCLS after LPS treatment were determined by RNA-seq. (I) The Venn diagram shows common and unique DEGs in PCLS treated with LPS in the presence of anti-human OSM-blocking antibody or an isotype control antibody. LPS-induced, OSM-dependent (J), and OSM-regulated (K) genes are shown. (**L**) Expression of OSM (top) and OSMR (bottom) on individual cell types is shown using scRNA-seq of healthy human lung tissue. tSNE, t-distributed Stochastic Neighbor Embedding; NK, natural killer; DC, dendritic cell. (**M** and **N**) LPS-induced OSM secretion from primary human MDMs (M) or mouse bone marrow–derived macrophages (BMDMs) (N) is shown. Data are presented as means ± SEM. Data were analyzed using Mann-Whitney tests. (**O**) The requirement of OSM from donor LPS-activated BMDM (top) and the requirement of OSM in recipient mice (bottom) were evaluated in vivo. i.t., intratracheal. (**P**) *Osm* expression was measured in isolated lung tissue from recipient C57BL/6 *Osm*$^{-/-}$ or C57BL/6 WT mice given WT or *Osm*$^{-/-}$ BMDM treated with LPS or PBS, as indicated. (**Q**) Expression of *Muc5ac*, *Il33*, *IL5*, *IL6*, *Il1b*, and *Il36g* was measured in isolated lung tissue in recipient C57BL/6*Osm*$^{-/-}$ or C57BL/6 WT mice given WT or *Osm*$^{-/-}$ BMDM treated with LPS or PBS, as indicated. $n = 5$ mice per group with one of two represents experiments shown. Data in (P) and (Q) are presented as FC relative to group 1. Means ± SEM are shown. Data were analyzed using Mann-Whitney tests. *$P < 0.05$.

These data indicate that OSM is an important and nonredundant component of the host response to bacterial LPS. To test whether OSM contributes to airway inflammatory responses after a live, metabolically active bacterial infection and whether OSM is necessary for antibacterial immunity, we infected WT mice with 10^4 *K. pneumoniae* and treated mice with anti-OSM or anti-gp120 control antibody. Anti-OSM–treated mice had significantly fewer airway neutrophils compared to anti-gp120–treated mice ($P < 0.05$; fig. S5A) and had significantly lower expression of *Muc5ac*, *Muc5b*, *Clca1/Gob5*, *Cxcl10*, and *Cxcl1* at multiple time points after infection ($P < 0.05$; fig. S5B). These data support an important and nonredundant role for OSM in bacterial-driven airway inflammation and mucus hypersecretion. *Il1a*, *Il1b*, and *Il6* were similar between anti-gp120– and anti-OSM–treated mice (fig. S5C), and there was no difference in bacterial colony-forming units per lung in anti-OSM–treated mice (fig. S5D). These data align with what we observed with LPS alone in WT versus *Osm*$^{-/-}$ mice (Fig. 6, A to E) and suggests that, although some inflammatory pathways are mediated by OSM, antibacterial immunity per se may not be compromised in the absence of OSM activity.

To test whether OSM contributed to LPS-induced responses in the human lung, we treated PCLSs obtained from healthy human donors with LPS for 4 (fig. S6A) or 24 hours (Fig. 6G) in the presence

or absence of anti-human OSM. As observed in murine lungs, LPS induced *OSM* in human PCLS (Fig. 6H) and led to both quantitative and qualitative transcriptional differences between PCLS treated with LPS or LPS + anti-OSM (Fig. 6I; $P < 0.05$). The overlap of LPS-induced, OSM-dependent genes in human PCLS and LPS-induced, OSM-dependent genes in mouse lung at 4 hours was very small (fig. S6A), which may be due to different cellular compositions between human PCLS and live mice, blocking function of commercially available anti-human OSM, or species differences including the use of OSMR and leukemia inhibitory factor receptor alpha (LIFR) with gp130 in human tissues, compared to OSMR and gp130 in mice. Nevertheless, many LPS-induced, OSM-dependent (Fig. 6J), and OSM-regulated (Fig. 6K) genes were identified in human PCLS. In particular, we identified OSM-dependent inflammatory genes [*CCL15*, *TNFRSF9* (*4-1BB*), *CCL2*, *CCL5*, *CCL7*, *CCL22*, *CCL24*, *CSF1*, *CD274* (*PDL1*), and *CD200*] and genes involved in microbial recognition and responsiveness (CD14 and TLR2) (Fig. 6J). Unlike preclinical murine studies (Fig. 6E), human OSM contributed to LPS-induced *IL1A*, *IL1B*, *CXCL10*, *CCL4*, and *CXCL3*, in addition to *IL19* and *CCL1* (Fig. 6K). Collectively, these data identify a previously underappreciated role for OSM in translating bacterial endotoxin recognition into inflammatory responses in both murine and human lung tissue.

Last, to identify putative LPS-responsive OSM-producing cells in the lung and to test how these cells could translate bacterial endotoxin recognition into inflammatory responses, we performed single-cell RNA sequencing (scRNA-seq) on fresh human lung tissue and identified macrophages as the dominant cell type expressing *OSM*, with BAEC and type II airway epithelial cells, smooth muscle cells, and fibroblasts (F) expressing the *OSMR* (Fig. 6L). Confirming previous reports, LPS potently induced OSM in human monocyte-derived macrophages (MDMs) and murine bone marrow–derived macrophages (BMDMs) (Fig. 6, M and N), suggesting that lung macrophages could be responsible for recognizing bacterial components and translating these into local inflammatory responses by the secretion of OSM. To test this hypothesis in vivo, we generated BMDM from WT and $Osm^{-/-}$ mice and treated them with phosphate-buffered saline (PBS) or LPS in vitro for 2 hours before adoptively transferring them into the lungs by intratracheal delivery (Fig. 6O). In lungs isolated 4 hours after macrophage transfer, *Osm* transcripts were significantly increased in mice receiving WT, but not $Osm^{-/-}$ BMDM, suggesting that transferred macrophages were the dominant source of *Osm* in this experimental system ($P < 0.05$; Fig. 6P). Mice receiving LPS-treated WT or $Osm^{-/-}$ BMDM showed comparable expression of *Il6*, *Il1b*, and *Il36g* in lung tissue; however, mice receiving WT BMDM showed significantly more *Muc5ac*, *Il33*, and *Il5* expression relative to mice receiving $Osm^{-/-}$ BMDM ($P < 0.05$; Fig. 6Q). Serum G-CSF and IL-5 were also significantly greater after infusion of WT BMDM, relative to $Osm^{-/-}$ BMDM ($P < 0.05$; fig. S6B), supporting the notion that macrophage-derived OSM is both necessary and sufficient to translate bacterial recognition into proallergic inflammatory responses.

DISCUSSION

Respiratory diseases including asthma are increasingly common and, at times, incapacitating. Acute exacerbations of disease, often leading to hospitalization with increased inflammation, mucus hypersecretion, and airway hyperreactivity, are approvable clinical endpoints for new therapeutics, highlighting the importance and impact of such events on patients' lives. Identifying the triggers of acute exacerbations, the molecular consequences of exposure to such triggers, and points of therapeutic intervention to prevent acute exacerbations is a major unmet need for people with asthma (*6*, *7*).

Opportunistic bacterial infections or microbial dysbiosis has been reported in a variety of airway diseases, including asthma (*8*–*10*, *12*, *58*), during influenza infections (*59*) and, more recently, in patients with severe coronavirus disease 2019 (COVID-19) (*60*). Furthermore, an endotoxin challenge can invoke an airway inflammatory response (*61*–*63*), supporting the hypothesis that bacterial infections may drive disease progression or acute exacerbations (*64*) in patients with asthma. Many allergens contain bacterial products, such as LPS (*13*) or LPS mimics (*14*) and preclinical models of asthma requiring LPS and LPS recognition receptors for allergen-induced airway inflammation (*15*, *16*), further supporting the notion that bacterial components contribute to the development, progression, and exacerbation of asthma. Responses to LPS have been extensively studied, particularly the induction of proinflammatory mediators such as IL-1α, IL-1β, TNF-α, and IL-8 (*21*). However, it has also been appreciated for many years that bacterial components induce OSM through a p38/mitogen-activated protein kinase–activated protein kinase 2–dependent pathway (*65*) with elevated plasma OSM correlating with plasma LPS in patients with severe COVID-19 (*60*). Despite these observations, it remained unclear whether OSM and bacterial-driven OSM contribute to the development, progression, or exacerbation of asthma and other inflammatory airway diseases.

OSM is elevated in a subset of patients with severe asthma (*24*, *26*), is secreted by a variety of immune cells observed in patients with asthma (*22*, *24*, *66*, *67*), and has been proposed as a disease biomarker (*68*). As we report here, OSM may also be a mechanistic contributor to disease pathogenesis. In this study, we provide evidence that LPS-induced OSM is a critical conduit, connecting bacterial exposure to many of the pathophysiological responses observed in severe asthma, including airway inflammation and mucus hypersecretion. Using ex vivo human biopsies from patients with asthma, scRNA-seq data from human lung biopsies, and primary human and mouse cells, we found that lung macrophages represent a major source of OSM and that OSM-driven responses in epithelial and mesenchymal cells recapitulate many key features observed in patients with severe asthma, including inflammatory and mucus-secreting responses. Supporting a scientific rationale for targeting OSM, we demonstrate using $Osm^{-/-}$ mice and an anti-OSM blocking antibody that OSM is an important nonredundant pathway in HDM, LPS, HDM + LPS, and *K. pneumoniae*–driven airway inflammation and mucus production. Mechanistically, using LPS-stimulated WT or *Osm*-deficient macrophages, we demonstrate that LPS drives OSM secretion from human and murine macrophages and that macrophage-derived OSM is both necessary and sufficient to induce local mucus production and local *Il33* expression and to invoke systemic granulocyte-recruiting responses, including G-CSF and IL-5.

OSM activates a variety of cells in the lung and induces many of the inflammatory and pathological features observed in severe asthma (*27*–*32*). In our cohort of patients with severe asthma, BAEC had elevated *OSMR*, *IL33*, and *SPDEF* expression, all of which are induced by OSM, supporting an OSM-driven feed-forward loop leading to inflammatory and mucus-producing pathways. Coupled with many observations reporting dysbiosis in patients with severe asthma (*64*), these data support a model where bacterial dysbiosis in the lung

of patients with asthma may be a key driver of OSM, contributing to disease progression.

Of the many factors induced by OSM, *IL33* was elevated in primary human airway epithelial cells, fibroblasts, and ASMs and has emerged as an attractive therapeutic target in asthma (*69*). In addition to its role in type 2 biology, IL-33 contributes to IL-13–independent (*70*) and non–type 2 airway responses (*71*), suggesting that signals beyond classical type 2 biology, including bacterial-associated signals, may be drivers of IL-33 in asthma. IL-33 and soluble interleukin 1 receptor like 1 (ST2), a receptor for IL-33, contribute to a variety of antibacterial responses (*72*), including LPS tolerance (*73*) and neutrophil migration during sepsis (*74*). Although *IL33* may be induced by a variety of factors beyond OSM, in both allergen- and LPS-driven airway inflammatory settings presented here, *Il33* induction was dependent on OSM, suggesting that OSM is a regulator of IL-33 in these settings. OSM-driven IL-33 in the lungs of mice, after administration of an adenovirus-encoding OSM, has previously been observed (*46*), but the dependency and requirement of physiological and endogenous OSM for IL-33 had not been established. Data presented here, demonstrating that LPS-induced IL-33 is dependent on OSM, identify OSM as an attractive therapeutic target for airway diseases where IL-33 has previously been implicated (*69*, *71*).

Mucus hypersecretion is a major disease trait in many patients with asthma, cystic fibrosis (CF), chronic obstructive pulmonary disease, and non-CF bronchiectasis, and identifying factors driving mucus hypersecretion has been a major focus for therapeutic intervention for many years (*75*). We observed that both mutant mice with a gain-of-function mutation in gp130 and $gp130^{F/F}$ and WT mice given exogenous rOSM had increased *Muc5ac* expression in the lung, suggesting that gp130 signaling and OSM contribute to mucus hypersecretion. Furthermore, using loss-of-function approaches, including $Osm^{-/-}$ mice, WT mice given anti-OSM blocking antibodies, or WT mice given $Osm^{-/-}$ macrophages, we demonstrated that airway mucus production was dependent on OSM and that macrophage-derived OSM may be an important source of OSM after LPS exposure. These data, and previous studies with adenoviral vectors overexpressing OSM leading to increased mucus (*54*), indicate that OSM both can contribute to mucus hypersecretion and is necessary for mucus secretion in allergen-exposed mice. However, these data do not identify whether OSM is a direct or indirect driver of mucus in the airways. Primary human BAECs grown at an ALI treated with OSM led to phosphorylation of STAT3, STAT4, and STAT5 within 15 min; up-regulated a suite of genes involved in goblet cell differentiation within 6 hours, including *MUC5B*, *BPIFB1*, *MUC1*, and *MUC4*; and adopted goblet cell staining characteristics with extracellular mucus secretion after 3 days and for up to 14 days. These data demonstrate that, in addition to IL-13 (*76*), OSM is a direct inducer of mucus secretion from airway epithelial cells adding to the appeal of OSM as a therapeutic target to treat inflammatory airway diseases associated with mucus hypersecretion.

IL-6 has been proposed as a therapeutic target for severe asthma (*77*). As we show here, OSM is also a potent inducer of *IL6* in primary human lung fibroblasts and ASMs. We also show that secretion of IL-6 into the airways of mice after HDM/LPS exposure is dependent on OSM. It has also previously been demonstrated that OSM-driven pulmonary inflammation is dependent on IL-6 (*78*). Although there are likely to be many drivers of IL-6, determining whether blocking OSM also reduces IL-6 in the clinic could identify an additional benefit of targeting OSM.

Our study has several limitations. Further studies should determine the expression of OSM in the BAL fluid, lung tissue, and plasma of patients with severe asthma during stable disease, during a bacterial-associated exacerbation of symptoms, and after the resolution of symptoms. Antagonizing OSM in the clinic has identified an important role for OSM in maintaining systemic platelet concentrations. Although this is dose dependent and reversible, close monitoring of platelets would be required.

Nevertheless, OSM blockade reduced many of the pathophysiological features associated with asthma in vitro and in vivo; however, OSM blockade did not affect critical antibacterial pathways such as IL-1α, IL-1β, and TNF-α (*21*) and did not compromise antibacterial immunity. Together, these results provide a scientific rationale supporting the clinical development of therapeutics targeting OSM to prevent asthma progression and bacterial-driven exacerbations of disease.

MATERIALS AND METHODS

Study design

The objective of this study was to identify pathways that may contribute to severe asthma from patient biopsies and to test these candidate using in vitro and in vivo preclinical models. For all experiments, the number of replicates and statistical test used are reported in the figure legends. The reported replicates refer to biological replicates. All in vitro experiments in the main text were performed at least three times, and no outliers or other data points were excluded. For in vivo experiments, cages of mice were randomly assigned to treatment groups. The scientists treating the mice were not blinded to the names of treatment groups.

Human clinical cohorts

Patients with moderate asthma and healthy controls were participants in the Study of the Mechanisms of Asthma (NCT00595153) (*79*). Biomarkers in Corticosteroid-refractory Asthma (BOBCAT) (*41*) was a multicenter observational study conducted in the United States, Canada, and the United Kingdom of 67 adult patients with moderate-to-severe asthma. Inclusion criteria required a diagnosis of moderate-to-severe asthma (confirmed by a forced expiratory volume in 1 s) between 40 and 80% of predicted value and evidence within the past 5 years of >12% reversibility of airway obstruction with a short-acting bronchodilator or methacholine sensitivity (PC20 < 8 mg/ml) that was uncontrolled [as defined by at least two exacerbations in the prior year or a score of >1.50 on the Asthma Control Questionnaire 5 (ACQ5) while receiving a stable dose regimen (>6 weeks) of a high dose of inhaled corticosteroids (>1000-μg fluticasone or equivalent per day)] with or without a long-acting β-agonist. Post hoc analysis of datasets generated from bronchial brushings from healthy controls or patients with moderate and severe asthma was performed using Ingenuity Pathway Analysis (IPA) (*42*).

Mice

C57BL/6 WT, C57BL/6 $Osm^{-/-}$ (C57BL/6N-A^{tm1Brd} $Osm^{tm1b(KOMP)Wtsi}$/JMmucd; Mutant Mouse Resource and Research centers (MMRRC) stock number 048921-UCD), and $gp130^{F/F}$ female mice (*53*), 4 to 8 weeks old, were used for our studies. Mice were kept in a standard 12-hour light/12-hour dark cycle under specific pathogen–free conditions and were allowed free access to sterile food and water. All mouse experimentation protocols were approved by the Laboratory

Animal Resources Committee at Genentech Inc. and adhered to the National Institutes of Health Guidelines for the Care and Use of Laboratory Animals.

In vivo PD and airway inflammation efficacy models

For PD studies, mice were treated with 24.A8 or isotype control antibody [20 mg/kg, intraperitoneally (ip)] on day 0, followed by 50 ng of recombinant murine OSM by the intratracheal route. After 15 min, mice were euthanized with lungs aseptically removed, and cell lysates were recovered and used for pSTAT3 assay using Meso Scale Discovery (MSD) assays, following the manufacturer's recommendations.

For acute HDM-induced airway inflammation, mice were anesthetized with an intraperitoneal injection of ketamine (40 mg/kg) with dexmedetomidine (1 mg/kg). Once anesthetized, mice were treated with HDM (Greer, 10 μg in 25 μl) by the intratracheal route. After HDM treatment, mice were administered an intraperitoneal injection of atipemazole (5 mg/kg) to accelerate recovery from anesthesia. Using a submaximal model to identify whether OSM could increase airway inflammation, mice were given HDM on days 0, 3, 7, 10, and 14 and analyzed on day 15 for airway infiltrates. In some experiments, mice were given HDM supplemented with recombinant murine OSM (50 ng) on days 10 and 14 and analyzed on day 15.

For models of established airway inflammation, mice were treated with HDM (Greer, 10 μg in 25 μl) on days 0, 2, 4, 14, 16, 28, and 30 and analyzed on day 31. In some experiments, mice were treated with HDM (Greer, 10 μg in 25 μl) supplemented with LPS (5 μg per mouse) on days 0, 2, 4, 14, 16, 28, and 30 and analyzed on day 31. For isolation of airway epithelial cells at day 31, mice were euthanized and perfused, and lungs are excised. Lungs were digested with collagenase, dispase II (Roche), and deoxyribonuclease 1 (DNase 1) (New England Biolabs), before washing, staining, and fluorescence-activated cell sorting (FACS). For histology, lungs were fixed in 10% neutral-buffered formalin, trimmed, processed, and paraffin-embedded, and 4-μm sections were stained with Alcian blue–periodic acid–Schiff (AB-PAS). Airway goblet cell hyperplasia severity was scored blinded to treatment group using a semiquantitative scale from 0 to 3, subjectively reflecting none, <25, 25 to 50, and >50% airway epithelial coverage by AB-PAS$^+$ goblet cells.

For LPS-induced airway responses, mice were anesthetized with an intraperitoneal injection of ketamine (40 mg/kg) with dexmedetomidine (1 mg/kg), given LPS (Sigma-Aldrich; 5 μg per mouse) by the intranasal route, and then given an intraperitoneal injection of atipemazole (5 mg/kg) to accelerate recovery from anesthesia. Mice were euthanized after 4 hours for analysis.

For *K. pneumoniae* infection studies, BALB/c mice were anesthetized with an intraperitoneal injection of ketamine (75 to 80 mg/kg) with xylazine (7.5 to 15 mg/kg), given 10^4 bacteria by the intranasal route, and treated with anti-OSM or anti-gp120 control antibody. Cohorts of mice were analyzed at 24, 72, and 168 hours after infection for airway inflammation, gene expression, and bacterial burden, as previously described (*80*).

For macrophage transfer experiments, BMDMs were generated from C57BL/6 WT or C57BL/6 *Osm*$^{-/-}$ mice, as described in the "Cell culture" section, and stimulated with LPS (50 ng/ml) or PBS in suspension. After 2 hours, BMDMs were washed three times with 10 volume washes of PBS before 1×10^6 BMDMs were transferred, by the intratracheal route in 25 μl, to anesthetized recipient C57BL/6 WT or C57BL/6 *Osm*$^{-/-}$ mice. After a further 4 hours, mice were euthanized.

In all experiments, mice were euthanized with pentobarbital sodium (390 mg/ml) and phenytoin sodium (50 mg/ml; Euthasol, Virbac Animal Health) (200 mg/kg) with blood recovered during terminal exsanguination. Serum was separated using serum separator tubes (Starstedt). Total BAL cells and differential cell counts were determined from two BAL washes. First, 500 μl of ice-cold PBS was used to lavage the airspaces for cellular and analyte analyses. A second lavage of 2 × 500 μl was used for additional cellular recovery. Lungs were recovered in RNAlater and stored at 4°C for 24 hours, before longer storage at −80°C before RNA recovery.

Reagents, Luminex, and pSTAT analysis

Human and murine chemokine and cytokine concentrations were assayed by Luminex technology using Bio-Plex Pro (Bio-Rad Laboratories) according to the manufacturer's instructions. Fluorescence intensities (FIs) from the labeled beads were read using FlexMaps instrument (Luminex Corp). FIs from diluted standards were used to construct standard curves using Bio-Plex Manager software (Bio-Rad Laboratories) using either 4- or 5-pl regression type. Data are presented as average of duplicate measurements. Recombinant human and mouse OSM was purchased from R&D Systems. Murine and human pSTAT3 (Tyr^{705}), pSTAT4 (Tyr^{693}), and pSTAT5a and pSTAT5b (Tyr^{694}) were measured in either murine lung tissue lysates 15 min after intratracheal delivery of rOSM, in MLg fibroblast cell lysates after treatment with rOSM with or without anti-OSM (24.A8), or in lysates from primary human BAECs, primary human fibroblasts, or primary human ASMs according to the manufacturer's instructions (MSD).

RNA-seq, scRNA-seq, IPA, and quantitative reverse transcription polymerase chain reaction

Tissue and cell samples were collected RNAlater (Qiagen) for storage or directly into TRIzol (Thermo Fisher Scientific) for processing. After tissue dissociation and lysis, lysates were mixed with chloroform and centrifuged at 13,000*g* for 15 min. The resulting aqueous phase was mixed with a 1.5× volume of absolute ethanol before purification using Qiagen RNeasy columns following the manufacturer's recommendations. RNA integrity was assessed using a bioanalyzer before RNA-seq or quantitative reverse transcription polymerase chain reaction. Purified RNA (100 ng) was reverse-transcribed using iScript (Bio-Rad) following the manufacturer's instructions, and the following TaqMan probes (Thermo Fisher Scientific) were used: murine *Muc5ac* (Mm01276718_m1), *Muc5b* (Mm00466391_m1), *Il33* (Mm00505403_m1), *Il5* (Mm00439646_m1), *Il6* (Mm00446190_m1), *Il1b* (Mm00434228_m1), *Il36g* (*Il1f9*)(Mm00463327_m1), and *Osmr* (Mm01307326_m1); human *OSM* (Hs00171165_m1). For RNA-seq, transcriptome profiles were generated using TruSeq RNA Access technology (Illumina). RNA-seq reads were processed using the HTSeqGenie R package (v.4.2.2). Briefly, RNA-seq reads were first aligned to ribosomal RNA sequences to remove ribosomal reads. The remaining reads were aligned to the mouse reference genome (GRCm38) using Genomic Short-read Nucleotide Alignment Program (GSNAP) (1, 2) version 2013-11-10, allowing a maximum of two mismatches per 75-base sequence (parameters: '-M 2 -n 10 -B 2 -i 1 -N 1 -w 200000 -E 1-pairmax-rna = 200000 –clip-overlap). To quantify gene expression, we counted the number of reads aligning within exons of gene models provided by GENCODE basic (v.27). We used the DESeq2 package (https://doi.org/10.1186/s13059-014-0550-8) to determine differential expression between test and control samples.

We used package defaults for size factor calculation, dispersion estimation, and model fitting.

Human scRNA-seq sample preparation, library construction, and analysis

After BAL, fresh lung tissue samples from transplant rejections were stored in complete media containing high-glucose Dulbecco's modified Eagle's medium (DMEM) with 10% heat-inactivated fetal bovine serum (FBS), 2 mM L-glutamine, and 0.5% penicillin-streptomycin on wet ice overnight. The tissue was washed in Hanks' balanced salt solution (HBSS) and then thoroughly minced in digestion buffer [HBSS; collagenase D (2.5 mg/ml) and DNAse (100 μg/ml)]. Minced tissue was rocked for 45 min at 37°C. Residual tissue material was transferred into fresh digestion buffer and rocked for another 45 min at 37°C. Single cells from both rounds of digest were combined and used for downstream analyses.

Single-cell preparations were labeled with a cocktail of fluorescently labeled antibodies including CD45 brilliant ultraviolet 421 (1:200 dilution; BD Biosciences, catalog no. 563792), EpCAM phycoerythrin (PE) (1:100 dilution; BD Biosciences, catalog no. 566841), CD31 PE-CY7 (1:100 dilution; BD Biosciences, catalog no. 563651), CD90 allophycocyanin (1:200 dilution; BD Biosciences, catalog no. 561971), and Live/Dead eFluor 780 (1:1000; Invitrogen, 65-0865-14) diluted in PBS containing 1% FBS for 20 min and then subjected to FACS to isolate specific populations. scRNA-seq library preparation was performed using the 10x Genomics Chromium platform with a Single Cell 3′ Library and Gel bead kit v2 following the manufacturer's user guide (10x Genomics). In brief, the cell density and viability of single-cell suspension were determined by a Vi-CELL XR cell counter (Beckman Coulter). All of the processed samples had high percentage of viable cells. The cell density was used to impute the volume of single-cell suspension needed in the reverse transcription master mix, aiming to achieve about 6000 cells per sample. Complementary DNAs and libraries were prepared following the manufacturer's user guide (10x Genomics). Libraries were profiled by a Bioanalyzer High-Sensitivity DNA kit (Agilent Technologies) and quantified using the Kapa Library Quantification Kit (Kapa Biosystems). Each library was sequenced in one lane of HiSeq 4000 (Illumina) following the manufacturer's sequencing specification (10x Genomics).

Sequencing reads were assembled and aligned against the GRCh38 human reference using Cell Ranger v3.0.2 (10x Genomics). Expression count matrices were analyzed using the Seurat v3.1 (*81*) R package (*82*). Only cells with ≥500 features and ≤5% total mitochondrial feature counts were retained for analysis. Normalization was performed using the log-normalization method. About 4000 highly variable features were selecting using the mean/variance regression method for sample integration and clustering after removal of immunoglobulin and T cell receptor variable domain features from the highly variable feature set. Sample integration and batch correction were performed using the anchor-based sample integration workflow. Clustering was performing using 20 principal components analysis components on a $k = 20$ shared nearest-neighbor (SNN) graph using the Louvain algorithm. Uniform manifold approximation and projection for dimensional reductions were performed using umap-learn v0.3.10 (*83*) on the same SNN graph used for clustering. Marker selection was performed using the Wilcoxon rank sum test on the integrated sample data for each cluster against all clusters. Cell type annotations were performed manually on the basis of inspection of canonical marker expression and differentially expressed cluster markers.

Cell culture

BAECs were purchased from Lonza (CC-2540S), expanded in bronchial epithelial growth media (CC-3170), and seeded on 6.5-mm Transwell plates in a humidified incubator at 37°C with 5% CO_2. After forming a confluent monolayer, media were lifted from the cells, and the media in the lower chamber were changed to pneumacult-ALI medium (Stem Cell Biotechnology, 05001) to allow cells to differentiate. After 21 days, beating cilia could be observed on 60 to 80% of the Transwell surface. BAEC-ALIs were then stimulated with recombinant human OSM (50 ng/ml) at this time (T0) and then collected at 6, 12, 24, 72, 168, and 336 hours after stimulation. For mucin area analysis and goblet cell count, BAEC-ALI cultures were fixed in 4% paraformaldehyde (PFA) for 15 min at room temperature, diluted to 1% PFA overnight, processed the following day, and embedded in paraffin. Four-micrometer sections were collected on glass slides and then stained overnight at 4°C with the following antibodies: anti-CC10 (Santa Cruz Biotechnology, sc-365992; 1:100 dilution), anti-Muc5b (Santa Cruz Biotechnology, sc-20119; 1:500), anti–acetylated tubulin (Santa Cruz Biotechnology, sc-23950; 1:400), and anti-Muc5ac (Thermo Fisher Scientific, MA1-38223; 1:100) before washing with PBS and secondary staining with donkey anti-goat Alexa Fluor 488 (AF488) (Invitrogen, A11055; 1:1000), donkey anti-rabbit AF647 (Invitrogen, A31573; 1:750), and donkey anti-mouse AF555 (Invitrogen, A31570; 1:1000). Slides were counterstained with 4′,6-diamidino-2-phenylindole mounted with Prolong hardset with images collected with an autostainer 360 (Thermo Fisher Scientific), and the area of the mucin-positive channel and the number of goblet cells (intact cells within the ciliated cell layer containing mucin) were normalized to the length of the permeable polycarbonate membrane on which the BAEC-ALI are grown using ImageJ software.

Fully differentiated BAEC-ALI cultures were treated with OSM at concentrations ranging from 0.1 ng/ml to 1 μg/ml for 7 days. Cultures were then incubated with PBS for 15 min at 37°C, and excess mucus and PBS were aspirated from the apical surface. On day 8, 50 μl of 2 μm of tetramethyl rhodamine isothiocyanate fluorescent beads (Thermo Fisher Scientific; diluted in PBS; 1:50,000) was added to the apical surface and allowed to settle into the mucus. Bead movement was imaged with a 4× Plan Fluor objective [numerical aperture, 0.13; Nikon] on a Nikon Ti-E inverted microscope equipped with a Neo Scientific Complementary metal–oxide–semiconductor (scMOS) camera (Andor), 37°C, 5% CO_2 environmental chamber (Okolab), all run by NIS Elements software (Nikon). Bead displacement was calculated and normalized as a percentage of maximum bead displacement in Imaris by spot tracking (Bitplane) and averaged across three wells.

NHLFs were purchased from Lonza (CC-2512) and cultured for a single passage in FGM-2 Fibroblast medium (CC-3132) before being incorporated into Lonza collagen rafts (200,000 cells per raft) per the manufacturer's instructions. Primary human ASMs were purchased from Lonza (CC-2576) and cultured for a single passage in SmGM-2 medium (CC-3182) before 30,000 cells were plated with Matrigel that had been defrosted overnight on wet ice and diluted 1:5 with SmGM-2 media. Matrigel was polymerized by placing the seeded constructs at 37°C, before 1 ml of complete SmGM-2 media was added 30 min later.

For generation of BMDM, bone marrow was recovered from the femur and tibia of adult mice and red blood cells lysed with cell lysis

buffer (Cell Signaling Technology). After lysis, bone marrow cells were cultured on non–cell culture–treated plates in DMEM supplemented with 10% FBS, GlutaMAX (Gibco), penicillin-streptomycin-glutamine (Thermo Fisher Scientific), and mouse macrophage colony-stimulating factor (M-CSF; 50 ng/ml; PeproTech). Suspended cells were removed with adherent cells provided with fresh medium on days 3 and 5. BMDM cells were harvested on days 7 to 10. BMDMs were stimulated with LPS (50 ng/ml; Sigma-Aldrich), where indicated.

For human MDMs, peripheral blood mononuclear cells were isolated from blood and cultured on non–cell culture–treated plates in DMEM containing 10% FBS, GlutaMAX (Gibco), and human M-CSF (50 ng/ml; PeproTech). Suspended cells were removed with adherent cells provided with fresh medium on days 3 and 5. Human MDMs were harvested on day 7.

Preparation of human PCLSs

Healthy whole lungs were received from the National Disease Research Interchange. The smallest lobe was cut free, exposing its main bronchiole, and inflated with 2% (w/v) low–melting point agarose solution. Once the agarose had solidified, the lobe was sectioned. Cores of 8 mm in diameter were made in which a small airway was visible. The cores were placed in a Krumdieck tissue slicer (Alabama Research & Development model no. MD4000), and the speed was set to produce slices at about 1 per 30 s. PCLSs (thickness, 250 μm) were transferred in sequence to wells containing Ham's F-12 medium to identify contiguous airway segments. Suitable airways on slices were selected on the basis of the following criteria: presence of a full smooth muscle wall (cut perpendicular to direction of airway), presence of beating cilia and internal folding of epithelium to eliminate blood vessels, and presence of unshared muscle walls at airway branch points to eliminate possible counteracting contractile forces. Slices were then incubated at 37°C on a rotating platform in a humidified air/CO_2 (95%/5%) incubator. PCLSs were cultured in complete DMEM and stimulated with LPS (1 μg/ml) with or without anti-human OSM (10 μg/ml; Clone 10G8).

Anti-OSM antibody generation and PK evaluation

The hybridoma-derived antibody 24.A8 was generated by immunizing hamsters with murine OSM. Then, the molecularly cloned antibody was reformatted into murine IgG2a for further studies. Binding kinetics were determined using surface plasmon resonance on a Biacore (Cytiva) instrument. The PKs of 24.A8 after single intravenous dose of 10 or 30 mg/kg were conducted at Charles River Laboratories, using naïve female C57BL/6 mice, age 6 to 8 weeks. Blood samples were collected by retro-orbital bleeds, and the terminal blood sample was collected by a cardiac stick from each animal in each dosing group at various time points up to 14 days after dose with three mice per time point and processed to collect serum. PK properties are shown in table S3. Serum samples were analyzed for test article concentrations by enzyme-linked immunosorbent assay. Mouse anti-mouse IgG2a (BD Biosciences) was used as the capturing reagent, and anti-mouse IgG2a-specific antibody conjugated to horseradish peroxidase (GeneTex) was used as the detection reagent. The serum concentration versus time data were used to calculate PK parameters in mouse using noncompartmental analysis (Phoenix WinNonlin, version 6.4.0.768; Certara). Nominal sample collection times and nominal dosing solution concentrations were used in the data analysis. Mouse anti-human OSM (clone 10G8) was used to block human OSM.

Statistical analysis

All raw, individual-level data are presented in data file S1. Statistical analysis was performed using GraphPad Prism v9 (GraphPad). Unless stated otherwise, data are presented as means ± SEM. Variable differences between two experimental groups were assessed using paired or unpaired *t* tests or Mann-Whitney tests, as indicated in figure legends. One-way analysis of variance (ANOVA) followed by Dunnett's test was used for comparisons of multiple treatment groups with the control group. *P* values were used to determine statistical significance and are shown in figure legends.

SUPPLEMENTARY MATERIALS

www.science.org/doi/10.1126/scitranslmed.abf8188
Figs. S1 to S6
Tables S1 to S3
Data file S1

View/request a protocol for this paper from *Bio-protocol*.

REFERENCES AND NOTES

1. J. V. Fahy, Type 2 inflammation in asthma—Present in most, absent in many. *Nat. Rev. Immunol.* **15**, 57–65 (2015).
2. K. F. Rabe, P. Nair, G. Brusselle, J. F. Maspero, M. Castro, L. Sher, H. Zhu, J. D. Hamilton, B. N. Swanson, A. Khan, J. Chao, H. Staudinger, G. Pirozzi, C. Antoni, N. Amin, M. Ruddy, B. Akinlade, N. M. H. Graham, N. Stahl, G. D. Yancopoulos, A. Teper, Efficacy and safety of dupilumab in glucocorticoid-dependent severe asthma. *N. Engl. J. Med.* **378**, 2475–2485 (2018).
3. H. G. Ortega, M. C. Liu, I. D. Pavord, G. G. Brusselle, J. M. FitzGerald, A. Chetta, M. Humbert, L. E. Katz, O. N. Keene, S. W. Yancey, P. Chanez, Mepolizumab treatment in patients with severe eosinophilic asthma. *N. Engl. J. Med.* **371**, 1198–1207 (2014).
4. J. Corren, R. F. Lemanske Jr., N. A. Hanania, P. E. Korenblat, M. V. Parsey, J. R. Arron, J. M. Harris, H. Scheerens, L. C. Wu, Z. Su, S. Mosesova, M. D. Eisner, S. P. Bohen, J. G. Matthews, Lebrikizumab treatment in adults with asthma. *N. Engl. J. Med.* **365**, 1088–1098 (2011).
5. W. Busse, J. Corren, B. Q. Lanier, M. McAlary, A. Fowler-Taylor, G. D. Cioppa, A. van As, N. Gupta, Omalizumab, anti-IgE recombinant humanized monoclonal antibody, for the treatment of severe allergic asthma. *J. Allergy Clin. Immunol.* **108**, 184–190 (2001).
6. G. L. Chupp, R. Kaur, A. Mainardi, New therapies for emerging endotypes of asthma. *Annu. Rev. Med.* **71**, 289–302 (2020).
7. GBD 2017 Disease and Injury Incidence and Prevalence Collaborators, Global, regional, and national incidence, prevalence, and years lived with disability for 328 diseases and injuries for 195 countries, 1990-2016: A systematic analysis for the Global Burden of Disease Study 2016. *Lancet* **390**, 1211–1259 (2017).
8. T. P. Wypych, L. C. Wickramasinghe, B. J. Marsland, The influence of the microbiome on respiratory health. *Nat. Immunol.* **20**, 1279–1290 (2019).
9. Q. Zhang, R. Illing, C. K. Hui, K. Downey, D. Carr, M. Stearn, K. Alshafi, A. Menzies-Gow, N. Zhong, K. Fan Chung, Bacteria in sputum of stable severe asthma and increased airway wall thickness. *Respir. Res.* **13**, 35 (2012).
10. Q. Zhang, M. Cox, Z. Liang, F. Brinkmann, P. A. Cardenas, R. Duff, P. Bhavsar, W. Cookson, M. Moffatt, K. F. Chung, Airway microbiota in severe asthma and relationship to asthma severity and phenotypes. *PLOS ONE* **11**, e0152724 (2016).
11. Y. J. Huang, S. Nariya, J. M. Harris, S. V. Lynch, D. F. Choy, J. R. Arron, H. Boushey, The airway microbiome in patients with severe asthma: Associations with disease features and severity. *J. Allergy Clin. Immunol.* **136**, 874–884 (2015).
12. M. A. Ghebre, P. H. Pang, S. Diver, D. Desai, M. Bafadhel, K. Haldar, T. Kebadze, S. Cohen, P. Newbold, L. Rapley, J. Woods, P. Rugman, I. D. Pavord, S. L. Johnston, M. Barer, R. D. May, C. E. Brightling, Biological exacerbation clusters demonstrate asthma and chronic obstructive pulmonary disease overlap with distinct mediator and microbiome profiles. *J. Allergy Clin. Immunol.* **141**, 2027–2036.e12 (2018).
13. J. W. McAlees, G. S. Whitehead, I. T. W. Harley, M. Cappelletti, C. L. Rewerts, A. M. Holdcroft, S. Divanovic, M. Wills-Karp, F. D. Finkelman, C. L. Karp, D. N. Cook, Distinct Tlr4-expressing cell compartments control neutrophilic and eosinophilic airway inflammation. *Mucosal Immunol.* **8**, 863–873 (2015).
14. A. Trompette, S. Divanovic, A. Visintin, C. Blanchard, R. S. Hegde, R. Madan, P. S. Thorne, M. Wills-Karp, T. L. Gioannini, J. P. Weiss, C. L. Karp, Allergenicity resulting from functional mimicry of a Toll-like receptor complex protein. *Nature* **457**, 585–588 (2009).

15. S. C. Eisenbarth, D. A. Piggott, J. W. Huleatt, I. Visintin, C. A. Herrick, K. Bottomly, Lipopolysaccharide-enhanced, toll-like receptor 4-dependent T helper cell type 2 responses to inhaled antigen. *J. Exp. Med.* **196**, 1645–1651 (2002).
16. H. Hammad, M. Chieppa, F. Perros, M. A. Willart, R. N. Germain, B. N. Lambrecht, House dust mite allergen induces asthma via Toll-like receptor 4 triggering of airway structural cells. *Nat. Med.* **15**, 410–416 (2009).
17. R. R. Schumann, S. R. Leong, G. W. Flaggs, P. W. Gray, S. D. Wright, J. C. Mathison, P. S. Tobias, R. J. Ulevitch, Structure and function of lipopolysaccharide binding protein. *Science* **249**, 1429–1431 (1990).
18. E. Hailman, H. S. Lichenstein, M. M. Wurfel, D. S. Miller, D. A. Johnson, M. Kelley, L. A. Busse, M. M. Zukowski, S. D. Wright, Lipopolysaccharide (LPS)-binding protein accelerates the binding of LPS to CD14. *J. Exp. Med.* **179**, 269–277 (1994).
19. A. Poltorak, X. He, I. Smirnova, M. Y. Liu, C. V. Huffel, X. du, D. Birdwell, E. Alejos, M. Silva, C. Galanos, M. Freudenberg, P. Ricciardi-Castagnoli, B. Layton, B. Beutler, Defective LPS signaling in C3H/HeJ and C57BL/10ScCr mice: mutations in Tlr4 gene. *Science* **282**, 2085–2088 (1998).
20. K. Takeda, T. Kaisho, S. Akira, Toll-like receptors. *Annu. Rev. Immunol.* **21**, 335–376 (2003).
21. R. Medzhitov, T. Horng, Transcriptional control of the inflammatory response. *Nat. Rev. Immunol.* **9**, 692–703 (2009).
22. T. Suda, K. Chida, A. Todate, K. Ide, K. Asada, Y. Nakamura, K. Suzuki, H. Kuwata, H. Nakamura, Oncostatin M production by human dendritic cells in response to bacterial products. *Cytokine* **17**, 335–340 (2002).
23. N. R. West, B. M. J. Owens, A. N. Hegazy, The oncostatin M-stromal cell axis in health and disease. *Scand. J. Immunol.* **88**, e12694 (2018).
24. K. L. Pothoven, J. E. Norton, L. A. Suh, R. G. Carter, K. E. Harris, A. Biyasheva, K. Welch, S. Shintani-Smith, D. B. Conley, M. C. Liu, A. Kato, P. C. Avila, Q. Hamid, L. C. Grammer III, A. T. Peters, R. C. Kern, B. K. Tan, R. P. Schleimer, Neutrophils are a major source of the epithelial barrier disrupting cytokine oncostatin M in patients with mucosal airways disease. *J. Allergy Clin. Immunol.* **139**, 1966–1978.e9 (2017).
25. H. J. Kang, J. S. Kang, S. H. Lee, S. J. Hwang, S. W. Chae, J. S. Woo, H.-M. Lee, Upregulation of oncostatin M in allergic rhinitis. *Laryngoscope* **115**, 2213–2216 (2005).
26. J. L. Simpson, K. J. Baines, M. J. Boyle, R. J. Scott, P. G. Gibson, Oncostatin M (OSM) is increased in asthma with incompletely reversible airflow obstruction. *Exp. Lung Res.* **35**, 781–794 (2009).
27. K. L. Pothoven, J. E. Norton, K. E. Hulse, L. A. Suh, R. G. Carter, E. Rocci, K. E. Harris, S. Shintani-Smith, D. B. Conley, R. K. Chandra, M. C. Liu, A. Kato, N. Gonsalves, L. C. Grammer III, A. T. Peters, R. C. Kern, P. J. Bryce, B. K. Tan, R. P. Schleimer, Oncostatin M promotes mucosal epithelial barrier dysfunction, and its expression is increased in patients with eosinophilic mucosal disease. *J. Allergy Clin. Immunol.* **136**, 737–746.e4 (2015).
28. D. A. Knight, N. Asokananthan, D. N. Watkins, N. L. A. Misso, P. J. Thompson, G. A. Stewart, Oncostatin M synergises with house dust mite proteases to induce the production of PGE_2 from cultured lung epithelial cells. *Br. J. Pharmacol.* **131**, 465–472 (2000).
29. K. Y. Nagahama, S. Togo, O. Holz, H. Magnussen, X. Liu, K. Seyama, K. Takahashi, S. I. Rennard, Oncostatin M modulates fibroblast function via signal transducers and activators of transcription proteins-3. *Am. J. Respir. Cell Mol. Biol.* **49**, 582–591 (2013).
30. A. K. Scaffidi, S. E. Mutsaers, Y. P. Moodley, R. J. McAnulty, G. J. Laurent, P. J. Thompson, D. A. Knight, Oncostatin M stimulates proliferation, induces collagen production and inhibits apoptosis of human lung fibroblasts. *Br. J. Pharmacol.* **136**, 793–801 (2002).
31. D. S. Faffe, L. Flynt, M. Mellema, T. R. Whitehead, K. Bourgeois, R. A. Panettieri Jr., E. S. Silverman, S. A. Shore, Oncostatin M causes VEGF release from human airway smooth muscle: Synergy with IL-1β. *Am. J. Physiol. Lung Cell. Mol. Physiol.* **288**, L1040–L1048 (2005).
32. D. S. Faffe, L. Flynt, M. Mellema, P. E. Moore, E. S. Silverman, V. Subramaniam, M. R. Jones, J. P. Mizgerd, T. Whitehead, A. Imrich, R. A. Panettieri Jr., S. A. Shore, Oncostatin M causes eotaxin-1 release from airway smooth muscle: Synergy with IL-4 and IL-13. *J. Allergy Clin. Immunol.* **115**, 514–520 (2005).
33. N. R. West, A. N. Hegazy, B. M. J. Owens, S. J. Bullers, B. Linggi, S. Buonocore, M. Coccia, D. Görtz, S. This, K. Stockenhuber, J. Pott, M. Friedrich, G. Ryzhakov, F. Baribaud, C. Brodmerkel, C. Cieluch, N. Rahman, G. Müller-Newen, R. J. Owens, A. A. Kühl, K. J. Maloy, S. E. Plevy; Oxford IBD Cohort Investigators, S. Keshav, S. P. L. Travis, F. Powrie, Oncostatin M drives intestinal inflammation and predicts response to tumor necrosis factor-neutralizing therapy in patients with inflammatory bowel disease. *Nat. Med.* **23**, 579–589 (2017).
34. S. H. Shin, S. K. Han, S. H. Jeong, W. K. Kim, Potential of oncostatin M to accelerate diabetic wound healing. *Int. Wound J.* **11**, 398–403 (2014).
35. A. F. Wahl, P. M. Wallace, Oncostatin M in the anti-inflammatory response. *Ann. Rheum. Dis.* **60** (Suppl. 3), iii75–iii80 (2001).
36. R. A. Lindberg, T. S. C. Juan, A. A. Welcher, Y. Sun, R. Cupples, B. Guthrie, F. A. Fletcher, Cloning and characterization of a specific receptor for mouse oncostatin M. *Mol. Cell. Biol.* **18**, 3357–3367 (1998).
37. P. G. Woodruff, H. A. Boushey, G. M. Dolganov, C. S. Barker, Y. H. Yang, S. Donnelly, A. Ellwanger, S. S. Sidhu, T. P. Dao-Pick, C. Pantoja, D. J. Erle, K. R. Yamamoto, J. V. Fahy, Genome-wide profiling identifies epithelial cell genes associated with asthma and with treatment response to corticosteroids. *Proc. Natl. Acad. Sci. U.S.A.* **104**, 15858–15863 (2007).
38. B. D. Modena, J. R. Tedrow, J. Milosevic, E. R. Bleecker, D. A. Meyers, W. Wu, Z. Bar-Joseph, S. C. Erzurum, B. M. Gaston, W. W. Busse, N. N. Jarjour, N. Kaminski, S. E. Wenzel, Gene expression in relation to exhaled nitric oxide identifies novel asthma phenotypes with unique biomolecular pathways. *Am. J. Respir. Crit. Care Med.* **190**, 1363–1372 (2014).
39. P. G. Woodruff, B. Modrek, D. F. Choy, G. Jia, A. R. Abbas, A. Ellwanger, J. R. Arron, L. L. Koth, J. V. Fahy, T-helper type 2-driven inflammation defines major subphenotypes of asthma. *Am. J. Respir. Crit. Care Med.* **180**, 388–395 (2009).
40. Y. Sun, I. Peng, J. D. Webster, E. Suto, J. Lesch, X. Wu, K. Senger, G. Francis, K. Barrett, J. L. Collier, J. D. Burch, M. Zhou, Y. Chen, C. Chan, J. Eastham-Anderson, H. Ngu, O. Li, T. Staton, C. Havnar, A. Jaochico, J. Jackman, S. Jeet, L. Riol-Blanco, L. C. Wu, D. F. Choy, J. R. Arron, B. S. M. Kenzie, N. Ghilardi, M. H. A. Ismaili, Z. Pei, J. De Voss, C. D. Austin, W. P. Lee, A. A. Zarrin, Inhibition of the kinase ITK in a mouse model of asthma reduces cell death and fails to inhibit the inflammatory response. *Sci. Signal.* **8**, ra122 (2015).
41. G. Jia, R. W. Erickson, D. F. Choy, S. Mosesova, L. C. Wu, O. D. Solberg, A. Shikotra, R. Carter, S. Audusseau, Q. Hamid, P. Bradding, J. V. Fahy, P. G. Woodruff, J. M. Harris, J. R. Arron; Bronchoscopic Exploratory Research Study of Biomarkers in Corticosteroid-refractory Asthma (BOBCAT) Study Group, Periostin is a systemic biomarker of eosinophilic airway inflammation in asthmatic patients. *J. Allergy Clin. Immunol.* **130**, 647–654.e10 (2012).
42. A. Kramer, J. Green, J. Pollard Jr., S. Tugendreich, Causal analysis approaches in ingenuity pathway analysis. *Bioinformatics* **30**, 523–530 (2014).
43. T. R. Hubler, J. G. Scammell, Intronic hormone response elements mediate regulation of FKBP5 by progestins and glucocorticoids. *Cell Stress Chaperones* **9**, 243–252 (2004).
44. S. Saglani, S. Lui, N. Ullmann, G. A. Campbell, R. T. Sherburn, S. A. Mathie, L. Denney, C. J. Bossley, T. Oates, S. A. Walker, A. Bush, C. M. Lloyd, IL-33 promotes airway remodeling in pediatric patients with severe steroid-resistant asthma. *J. Allergy Clin. Immunol.* **132**, 676–685.e13 (2013).
45. D. Préfontaine, S. Lajoie-Kadoch, S. Foley, S. Audusseau, R. Olivenstein, A. J. Halayko, C. Lemière, J. G. Martin, Q. Hamid, Increased expression of IL-33 in severe asthma: Evidence of expression by airway smooth muscle cells. *J. Immunol.* **183**, 5094–5103 (2009).
46. C. D. Richards, L. Izakelian, A. Dubey, G. Zhang, S. Wong, K. Kwofie, A. Qureshi, F. Botelho, Regulation of IL-33 by oncostatin M in mouse lung epithelial cells. *Mediators Inflamm.* **2016**, 9858374 (2016).
47. G. Chen, T. R. Korfhagen, Y. Xu, J. Kitzmiller, S. E. Wert, Y. Maeda, A. Gregorieff, H. Clevers, J. A. Whitsett, SPDEF is required for mouse pulmonary goblet cell differentiation and regulates a network of genes associated with mucus production. *J. Clin. Invest.* **119**, 2914–2924 (2009).
48. J. M. Drazen, H. A. Boushey, S. T. Holgate, M. Kaliner, P. O'Byrne, M. Valentine, J. H. Widdicombe, A. Woolcock, The pathogenesis of severe asthma: A consensus report from the Workshop on Pathogenesis. *J. Allergy Clin. Immunol.* **80**, 428–437 (1987).
49. Y. Y. Koh, Y. W. Kim, J. D. Park, J. W. Oh, A comparison of serum haptoglobin levels between acute exacerbation and clinical remission in asthma. *Clin. Exp. Allergy* **26**, 1202–1209 (1996).
50. K. Samitas, E. Zervas, S. Vittorakis, M. Semitekolou, T. Alissafi, A. Bossios, H. Gogos, E. Economidou, J. Lotvall, G. Xanthou, V. Panoutsakopoulou, M. Gaga, Osteopontin expression and relation to disease severity in human asthma. *Eur. Respir. J.* **37**, 331–341 (2011).
51. P. R. Sears, W. N. Yin, L. E. Ostrowski, Continuous mucociliary transport by primary human airway epithelial cells in vitro. *Am. J. Physiol. Lung Cell. Mol. Physiol.* **309**, L99–L108 (2015).
52. V. Delimpoura, P. Bakakos, E. Tseliou, V. Bessa, G. Hillas, D. C. M. Simoes, S. Papiris, S. Loukides, Increased levels of osteopontin in sputum supernatant in severe refractory asthma. *Thorax* **65**, 782–786 (2010).
53. N. C. Tebbutt, A. S. Giraud, M. Inglese, B. Jenkins, P. Waring, F. J. Clay, S. Malki, B. M. Alderman, D. Grail, F. Hollande, J. K. Heath, M. Ernst, Reciprocal regulation of gastrointestinal homeostasis by SHP2 and STAT-mediated trefoil gene activation in gp130 mutant mice. *Nat. Med.* **8**, 1089–1097 (2002).
54. D. K. Fritz, C. Kerr, R. Fattouh, A. Llop-Guevara, W. I. Khan, M. Jordana, C. D. Richards, A mouse model of airway disease: Oncostatin M-induced pulmonary eosinophilia, goblet cell hyperplasia, and airway hyperresponsiveness are STAT6 dependent, and interstitial pulmonary fibrosis is STAT6 independent. *J. Immunol.* **186**, 1107–1118 (2011).
55. J. Huang, H. Yue, T. Jiang, J. Gao, Y. Shi, B. Shi, X. Wu, X. Gou, IL-31 plays dual roles in lung inflammation in an OVA-induced murine asthma model. *Biol. Open* **8**, bio036244 (2019).
56. W. C. Moore, A. T. Hastie, X. Li, H. Li, W. W. Busse, N. N. Jarjour, S. E. Wenzel, S. P. Peters, D. A. Meyers, E. R. Bleecker; National Heart, Lung, and Blood Institute's Severe Asthma

Research Program, Sputum neutrophil counts are associated with more severe asthma phenotypes using cluster analysis. *J. Allergy Clin. Immunol.* **133**, 1557–1563.e5 (2014).
57. S.-C. Liao, Y.-C. Cheng, Y.-C. Wang, C.-W. Wang, S.-M. Yang, C.-K. Yu, C.-C. Shieh, K.-C. Cheng, M.-F. Lee, S.-R. Chiang, J.-M. Shieh, M.-S. Chang, IL-19 induced Th2 cytokines and was up-regulated in asthma patients. *J. Immunol.* **173**, 6712–6718 (2004).
58. R. P. Dickson, F. J. Martinez, G. B. Huffnagle, The role of the microbiome in exacerbations of chronic lung diseases. *Lancet* **384**, 691–702 (2014).
59. R. K. Gupta, R. George, J. S. Nguyen-Van-Tam, Bacterial pneumonia and pandemic influenza planning. *Emerg. Infect. Dis.* **14**, 1187–1192 (2008).
60. P. S. Arunachalam, F. Wimmers, C. K. P. Mok, R. A. P. M. Perera, M. Scott, T. Hagan, N. Sigal, Y. Feng, L. Bristow, O. T.-Y. Tsang, D. Wagh, J. Coller, K. L. Pellegrini, D. Kazmin, G. Alaaeddine, W. S. Leung, J. M. C. Chan, T. S. H. Chik, C. Y. C. Choi, C. Huerta, M. P. McCullough, H. Lv, E. Anderson, S. Edupuganti, A. A. Upadhyay, S. E. Bosinger, H. T. Maecker, P. Khatri, N. Rouphael, M. Peiris, B. Pulendran, Systems biological assessment of immunity to mild versus severe COVID-19 infection in humans. *Science* **369**, 1210–1220 (2020).
61. M. W. Eldridge, D. B. Peden, Allergen provocation augments endotoxin-induced nasal inflammation in subjects with atopic asthma. *J. Allergy Clin. Immunol.* **105**, 475–481 (2000).
62. R. Rylander, B. Bake, J. J. Fischer, I. M. Helander, Pulmonary function and symptoms after inhalation of endotoxin. *Am. Rev. Respir. Dis.* **140**, 981–986 (1989).
63. O. Michel, J. Duchateau, R. Sergysels, Effect of inhaled endotoxin on bronchial reactivity in asthmatic and normal subjects. *J. Appl. Physiol. (1985)* **66**, 1059–1064 (1989).
64. K. F. Chung, Airway microbial dysbiosis in asthmatic patients: A target for prevention and treatment? *J. Allergy Clin. Immunol.* **139**, 1071–1081 (2017).
65. C. Ehlting, O. Böhmer, M. J. Hahnel, M. Thomas, U. M. Zanger, M. Gaestel, W. T. Knoefel, J. Schulte am Esch, D. Häussinger, J. G. Bode, Oncostatin M regulates SOCS3 mRNA stability via the MEK-ERK1/2-pathway independent of p38(MAPK)/MK2. *Cell. Signal.* **27**, 555–567 (2015).
66. M. Eberl, G. W. Roberts, S. Meuter, J. D. Williams, N. Topley, B. Moser, A rapid crosstalk of human γδ T cells and monocytes drives the acute inflammation in bacterial infections. *PLOS Pathog.* **5**, e1000308 (2009).
67. P. Salamon, N. G. Shoham, I. Puxeddu, Y. Paitan, F. Levi-Schaffer, Y. A. Mekori, Human mast cells release oncostatin M on contact with activated T cells: Possible biologic relevance. *J. Allergy Clin. Immunol.* **121**, 448–455.e5 (2008).
68. M. Hoggard, R. G. Douglas, M. W. Taylor, K. Biswas, Assessing tissue transcription biomarkers of chronic rhinosinusitis: A comparison of sampling methodologies. *Int. Forum Allergy Rhinol.* **10**, 1057–1064 (2020).
69. C. Donovan, P. M. Hansbro, IL-33 in chronic respiratory disease: From preclinical to clinical studies. *ACS Pharmacol. Transl. Sci.* **3**, 56–62 (2020).
70. V. Ramirez-Carrozzi, A. Sambandam, M. Zhou, D. Yan, J. Kang, X. Wu, E. Suto, M. Baca, C. Austin, M. Xu, W. Lee, R. Pappu, Combined blockade of the IL-13 and IL-33 pathways leads to a greater inhibition of type 2 inflammation over inhibition of either pathway alone. *J. Allergy Clin. Immunol.* **139**, 705–708.e6 (2017).
71. J. Kearley, J. S. Silver, C. Sanden, Z. Liu, A. A. Berlin, N. White, M. Mori, T.-H. Pham, C. K. Ward, G. J. Criner, N. Marchetti, T. Mustelin, J. S. Erjefalt, R. Kolbeck, A. A. Humbles, Cigarette smoke silences innate lymphoid cell function and facilitates an exacerbated type I interleukin-33-dependent response to infection. *Immunity* **42**, 566–579 (2015).
72. O. Rostan, M. I. Arshad, C. Piquet-Pellorce, F. Robert-Gangneux, J.-P. Gangneux, M. Samson, Crucial and diverse role of the interleukin-33/ST2 axis in infectious diseases. *Infect. Immun.* **83**, 1738–1748 (2015).
73. E. K. Brint, D. Xu, H. Liu, A. Dunne, A. N. J. McKenzie, L. A. J. O'Neill, F. Y. Liew, ST2 is an inhibitor of interleukin 1 receptor and Toll-like receptor 4 signaling and maintains endotoxin tolerance. *Nat. Immunol.* **5**, 373–379 (2004).
74. J. C. Alves-Filho, F. Sônego, F. O. Souto, A. Freitas, W. A. Verri Jr., M. Auxiliadora-Martins, A. Basile-Filho, A. N. McKenzie, D. Xu, F. Q. Cunha, F. Y. Liew, Interleukin-33 attenuates sepsis by enhancing neutrophil influx to the site of infection. *Nat. Med.* **16**, 708–712 (2010).
75. E. V. Ha, D. F. Rogers, Novel therapies to inhibit mucus synthesis and secretion in airway hypersecretory diseases. *Pharmacology* **97**, 84–100 (2016).
76. D. A. Kuperman, X. Huang, L. L. Koth, G. H. Chang, G. M. Dolganov, Z. Zhu, J. A. Elias, D. Sheppard, D. J. Erle, Direct effects of interleukin-13 on epithelial cells cause airway hyperreactivity and mucus overproduction in asthma. *Nat. Med.* **8**, 885–889 (2002).
77. M. C. Peters, K. W. McGrath, G. A. Hawkins, A. T. Hastie, B. D. Levy, E. Israel, B. R. Phillips, D. T. Mauger, S. A. Comhair, S. C. Erzurum, M. W. Johansson, N. N. Jarjour, A. M. Coverstone, M. Castro, F. Holguin, S. E. Wenzel, P. G. Woodruff, E. R. Bleecker, J. V. Fahy; National Heart, Lung, and Blood Institute Severe Asthma Research Program, Plasma interleukin-6 concentrations, metabolic dysfunction, and asthma severity: A cross-sectional analysis of two cohorts. *Lancet Respir. Med.* **4**, 574–584 (2016).
78. F. M. Botelho, J. Rangel-Moreno, D. Fritz, T. D. Randall, Z. Xing, C. D. Richards, Pulmonary expression of oncostatin M (OSM) promotes inducible BALT formation independently of IL-6, despite a role for IL-6 in OSM-driven pulmonary inflammation. *J. Immunol.* **191**, 1453–1464 (2013).
79. L. J. Simpson, S. Patel, N. R. Bhakta, D. F. Choy, H. D. Brightbill, X. Ren, Y. Wang, H. H. Pua, D. Baumjohann, M. M. Montoya, M. Panduro, K. A. Remedios, X. Huang, J. V. Fahy, J. R. Arron, P. G. Woodruff, K. M. Ansel, A microRNA upregulated in asthma airway T cells promotes TH2 cytokine production. *Nat. Immunol.* **15**, 1162–1170 (2014).
80. P. A. Smith, M. F. T. Koehler, H. S. Girgis, D. Yan, Y. Chen, Y. Chen, J. J. Crawford, M. R. Durk, R. I. Higuchi, J. Kang, J. Murray, P. Paraselli, S. Park, W. Phung, J. G. Quinn, T. C. Roberts, L. Rougé, J. B. Schwarz, E. Skippington, J. Wai, M. Xu, Z. Yu, H. Zhang, M. W. Tan, C. E. Heise, Optimized arylomycins are a new class of Gram-negative antibiotics. *Nature* **561**, 189–194 (2018).
81. T. Stuart, A. Butler, P. Hoffman, C. Hafemeister, E. Papalexi, W. M. Mauck III, Y. Hao, M. Stoeckius, P. Smibert, R. Satija, Comprehensive Integration of Single-Cell Data. *Cell* **177**, 1888–1902.e21 (2019).
82. R Core Team, *R: A Language and Environment for Statistical Computing* (R Foundation for Statistical Computing, 2020).
83. L. McInnes, J. Healy, J. Melville, UMAP: Uniform Manifold Approximation and Projection for Dimension Reduction. arXiv:1802.03426v3 (2018).

Acknowledgments: We thank M. Taylor (PTPK, Genentech) and P. Chan (BCP, Genentech) for assistance with PK analysis of anti-mouse OSM (24.A8). We are indebted to the guidance, assistance, and consultation with G. Nakamura (Antibody Discovery, Genentech). We would like to thank the vet staff at Genentech, C. Sohn, D. Montoya, R. Garcia-Gonzalez, E. Chua, J. Yamada, K. McEachin, R. Scott, F. Guardado, and J. Cosino, for the meticulous care and support for all animal work. We thank the Next Generation Sequencing group, Genentech, for all the assistance, guidance, and support with RNA sequencing. **Funding:** P.J.W. was funded by the National Health and Medical Research Council (NHMRC) of Australia Grants: Project Grant (APP1139371), Senior Medical Research Fellowship (APP1154279). R.A.P. is funded by NIH grants: NCATS UL1TR003017 and NHLBI PO1HL114471. B.J.J. is funded by The Nina Ireland Program for Lung Health. All other authors are funded by Genentech Inc. **Author contributions:** S.E.H., H.S.D., D.X., R.A.R., G.T., C.J.W., R.G. Y.S., J.W., D.Y. J.K., K.G., E.V.N., S.G., and Y.S. helped design and execute in vitro and in vivo assays and experiments. D.L. and C.E. helped optimize human BAEC-ALI (Fig. 2G and fig. S1C), fibroblast, and ASM culture conditions. D.J.D., K.B.M., P.J.W., and J.R.A. helped with sourcing, processing, and prepping human tissue for scRNA-seq (Fig. 6L). A.H., J.M., S.F., S.H., and V.N. assisted with all necropsy from in vivo experiments (Figs. 3 to 6). V.R.-C., R.P., and J.B helped generate and characterize anti-mouse OSM (24.A8) (Fig. 5). Y.C., C.C., A.A, J.V.-H., D.F.C., D.L., and M.X. helped design experiments, source and analyze human transcriptional data sets, and analyze RNA sequencing data (Figs. 1, 2, and 6). R.Y. carried out and analyzed PK studies with 24.A8 (Fig. 5F). C.A. analyzed pathology. Z.M. helped with experimental design, execution, and interpretation of RNA sequencing (Figs. 1, 2, and 6). R.A.P., C.K.-W., and W.F.J. sourced and provided PCLSs (Fig. 6, G to K). B.J.J. provided gp130^{Y757F} mice. J.E.K. and N.R.W. helped design experiments, provided reagents, and provided guidance. M.S.W. helped with experimental design, execution, and interpretation of the project and prepared the manuscript with input from all authors. **Competing interests:** All authors, except R.A.P., C.K.-W., W.F.J., B.J.J., and P.J.W., are current or past employees of Genentech Inc., a member of the Roche group, and may hold Roche stock or stock options. C.K.-W. is a coeditor in chief for Current Research in Pharmacology and Drug Discovery. **Data and materials availability:** All data associated with this study are present in the paper or the Supplementary Materials. Anti-mouse OSM antibody will be made available by contacting the corresponding author and completion of a material transfer agreement.

Submitted 21 November 2020
Resubmitted 30 July 2021
Accepted 1 December 2021
Published 12 January 2022
10.1126/scitranslmed.abf8188

Abstract

One-sentence summary: Bacterial-associated LPS drives oncostatin M–dependent airway inflammation and mucus hypersecretion in severe asthma.

Editor's Summary:
Addressing asthma

Severe asthma is thought to be driven by bacterial dysbiosis, but the mechanism linking the two remains unclear. Headland *et al.* sought to understand this mechanism, identifying oncostatin M as a mediator of severe asthma. Blocking oncostatin M with an antibody reduced severe asthma-related symptoms in mice after exposure to bacterial stimuli. Together, these findings support further development of antibodies and other drugs targeting oncostatin M as a treatment for severe asthma.